

OAK RIDGE NATIONAL LABORATORY LIBRARIES



3 4456 0555856 2

ORNL/TM-5550  
(Part II of ORNL/TM-5534)

*Cy 85*

**Effect of Steam Corrosion on HTGR Core  
Support Post Strength Loss: Part II.  
Consequences of Steam Generator  
Tube Rupture Event**

R. P. Wichner

**OAK RIDGE NATIONAL LABORATORY**

OPERATED BY UNION CARBIDE CORPORATION FOR THE ENERGY RESEARCH AND DEVELOPMENT ADMINISTRATION

OFFICE OF THE ATTORNEY GENERAL  
STATE OF MICHIGAN  
LANSING, MICHIGAN  
MAY 14 1968

Dear Sirs: I am writing to you regarding the Michigan  
State Police. I am sure you are aware of the fact that  
the Michigan State Police is a law enforcement agency  
and as such is subject to the provisions of the Michigan  
Public Employment Relations Act. I am sure you are  
also aware of the fact that the Michigan State Police  
is a public employer and as such is subject to the  
provisions of the Michigan Public Employment Relations  
Act.

ORNL/TM-5550  
(Part II of ORNL/TM-5534)  
Dist. Category UC-77

Contract No. W-7405-eng-26

CHEMICAL TECHNOLOGY DIVISION

EFFECT OF STEAM CORROSION ON HTGR CORE SUPPORT POST STRENGTH LOSS:

PART II. CONSEQUENCES OF STEAM GENERATOR TUBE RUPTURE EVENT

R. P. Wichner

Date Published: January 1977

OAK RIDGE NATIONAL LABORATORY  
Oak Ridge, Tennessee 37830  
operated by  
UNION CARBIDE CORPORATION  
for the  
ENERGY RESEARCH AND DEVELOPMENT ADMINISTRATION

OAK RIDGE NATIONAL LABORATORY LIBRARIES



3 4456 0555856 2



## TABLE OF CONTENTS

	<u>Page</u>
ABSTRACT .....	1
1. INTRODUCTION AND SUMMARY .....	2
1.1 Introduction .....	2
1.2 Summary of Results .....	3
2. DESCRIPTIONS AND TEMPERATURE HISTORIES OF POSTULATED ACCIDENT EVENTS .....	6
2.1 Description of Postulated Tube Rupture Events .....	6
2.2 Temperature Transients During Postulated Accidents Calculated by ORECA-3 .....	7
2.3 Assumed Moisture Ingress Rates Following Tube Failure .....	14
3. GRAPHITE CORROSION RATES DURING STEAM GENERATOR TUBE RUPTURE EVENTS .....	16
3.1 Steam Corrosion of Experimental Gas-Cooled Reactor (ECGR) Graphite by Helms and MacPherson .....	17
3.2 Experiments of Johnstone, Chen, and Scott .....	19
3.3 High-Pressure Experiments of Blackwood and McGrory ...	21
3.4 Comparison of Corrosion Rate Expressions in the High Steam Pressure Regime .....	23
3.5 Selection of Corrosion Rate Expressions Used in This Study .....	27
4. METHOD OF CALCULATION. OXIDO PROGRAM .....	29
4.1 OXIDO Program Description .....	29
4.2 Calculation of Core Post Burnoff and Strength Loss ...	32
5. CORE POST STRENGTH LOSS ESTIMATES .....	33
5.1 Strength Loss Estimates for the Nominal Core Post Supporting Zones 9, 11, and 67 .....	33
5.2 Effect of Localized Temperature Excess on Estimated Strength Loss .....	45
5.2.1 Hot Spots in the Core Support Post at Steady State .....	47
5.2.2 Core Post Hot Spots During Tube Burst Shutdown Transients .....	48
6. REFERENCES .....	50



EFFECT OF STEAM CORROSION ON HTGR CORE SUPPORT POST STRENGTH LOSS:II. CONSEQUENCES OF STEAM GENERATOR TUBE RUPTURE EVENTS

R. P. Wichner

## ABSTRACT

This report presents the concluding portion of a two-part study on the effect of steam corrosion on the strength of the graphite support posts of a High-Temperature Gas-Cooled Reactor. The first phase of the study dealt with long-term effects resulting from leakages from the steam generator that were sufficiently small to allow normal operation, whereas this concluding report treats the effects of infrequent tube-rupture events.

To perform the assessment, a series of eight tube-rupture events of varying severity and probability were postulated. Case 1 pertains to the situation where the moisture detection, loop isolation, and dump procedures function as planned; the remaining seven cases suppose various defects in the moisture detection system, the core auxiliary coolant system, and the integrity of the prestressed concrete reactor vessel. Core-graphite temperature histories were approximated for each type of event using the ORECA code. These were used in conjunction with the estimated steam ingress and graphite corrosion rates to obtain the impurity composition in the coolant during the shutdown procedure.

Core post burnoffs beneath three typical fuel zones were estimated for each postulated event from the determined impurity compositions and core post temperature history. Two separate corrosion rate expressions were assumed, as deemed most appropriate of those published for the high-oxidant level typical in tube rupture events. Core post strength losses were estimated from these burnoffs via a procedure adapted from Part I of this study. It was found that the nominal core post beneath the highest power factor fuel zone would lose from 0.02 to 2.5% of their strength, depending on an assumed corrosion rate equation and the severity of the event.

The effect of hot streaking during cooldown was determined by using preliminary estimates of its magnitude. It was found that localized strength loss beneath the highest power factor zone ranges from 0.23 to 1.2%, assuming reasonably probable hot-streaking circumstances. The combined worst case, hot streaking typical for a load-following transient and most severe

accident sequence, yields an estimated strength loss of from 25 to 33% for localized regions beneath the highest power factor zones.

---

## 1. INTRODUCTION AND SUMMARY

### 1.1 Introduction

This report deals with the effect of steam generator tube rupture events on the corrosion and consequent strength loss of the graphite core support posts\* employed in the High-Temperature Gas-Cooled Reactor (HTGR). As such, it forms the second and concluding part of a study on steam corrosion effects on the core support structure; the first part<sup>1</sup> was concerned with the effect of long-term steam inleakages of a sufficiently low level so as to allow normal reactor operation. Although the corrosion conditions are quite different in this second part of the study, the calculational methods employed are essentially modified versions of those used in the earlier study. Most important, the graphite strength-loss model used here is a direct adaptation of that developed in Sect. 6 of ref. 1, with only slight alterations to account for transient temperature conditions. The reader should therefore refer to the earlier study for full discussion of the graphite strength-loss model. The reference reactor selected for this study was basically the 3,000 MW(t) station described by the General Atomic Standard Safety Analysis Report (GASSAR-6),<sup>2</sup> with the exception that the newer core post diameter of 19.1 cm (7.5 in.) was used instead of the older value of 15.2 cm (6 in.).

A major difference between this and the earlier study is the form of the graphite corrosion equation selected from the analysis. Tube-burst events result in steam concentrations that peak at from 1.5 to 12.0-atm partial pressure compared with a maximum of about  $5 \times 10^{-4}$  atm allowed

---

\* Core post strength refers in this report to the compressive strength of the support post body. Effects of localized contact stresses at each end of the post are excluded.

for normal operations. There are far fewer studies at these higher partial-pressure conditions; hence, graphite corrosion rates during the transient shutdown conditions following major tube failure are less certain than for steady operation with lower levels of oxidant. A comparison of three high-steam, partial-pressure corrosion studies is presented in Sect. 3. Two of these were incorporated into the computer program used in the analysis, termed  $\phi$ XIDO, and the calculations are in parallel for comparison purposes.

The basic approach of this study was (1) to select a series of eight specific accident scenarios, (2) to obtain coolant and core graphite temperature histories for each event, and (3) to approximate the corrosion environment around the core posts during each event, (4) which would then be used to determine the burnoff and strength loss over the period of the shutdown transient. The postulated events, which cover a wide range of probability and severity are outlined in Sect. 2. Estimation of the likelihood of each event is not in the scope for this study; the strength loss results that are given are the values estimated to occur as a result of each event, assuming that it will occur.

The required temperature histories were obtained using the ORECA program employing as the starting point the given steady-state power distributions for the 3,000 MW(t), Fulton Generating Station operating at 105% of rated power. The core posts beneath three refueling zones were selected for study to represent, respectively, a high radial power factor, an average, and a peripheral refueling zone. The degree to which hot streaking may cause localized areas of high strength loss beneath the high radial power factor zone was estimated.

## 1.2 Summary of Results

The principal conclusions of this study are given in Table 1.1, which lists the anticipated range of support post strength loss beneath the high radial power factor fuel zone for each assumed accident situation. This table applies to the nominal core posts; that is, hot streaking effects are omitted. Two additional core post locations that were

Table 1.1. Predicted strength loss of nominal post beneath high-power factor zone for a series of eight assumed tube-burst accidents

Accident case <sup>a</sup>	Maximum developed partial pressure (atm)		Predicted strength loss (%) nominal post beneath high power factor zone
	H <sub>2</sub> O	H <sub>2</sub> , CO	
1	2.2	0.08 - 0.02 <sup>b</sup>	0.042 - 0.007 <sup>b</sup>
2	9.0	0.3 - 0.05	0.26 - 0.088
3	12.0	1.0 - 0.3	1.2 - 1.6
3A	12.0	2.5 - 0.8	2.4 - 1.9
4	1.5	0.07 - 0.01	0.043 - 0.008
5	4.0	0.7 - 0.4	0.43 - 0.40
6	2.4	0.7 - 0.4	0.26 - 0.13
6A	3.9	0.6 - 0.3	0.22 - 0.076

<sup>a</sup>Accident cases are fully described in Sect. 2.1.

<sup>b</sup>First value obtained using Helms-MacPherson corrosion equation;<sup>10</sup> second value assumes Johnstone, Chen, and Scott corrosion equation.<sup>11</sup>

examined — an average power factor zone and a peripheral zone — each showed less strength loss than is shown in Table 1.1. For accident Case 1, where proper functioning of the moisture monitor, loop isolation, and dump systems is assumed, the predicted strength loss of the nominal posts below the high-power fuel zone ranges from 0.042 to 0.007%. The range is obtained by using two estimates of the graphite corrosion rate under the shutdown transient conditions.

Accident Case 2 assumes failure of the moisture detection system and cooldown on the three auxiliary coolant loops. Higher steam pressures are experienced (briefly to 9 atm) because failure to isolate the leaking steam generator allows its contents to be discharged into the primary system. The predicted strength loss range for this case is 0.26 to 0.088%.

Cases 3 and 4 assume malfunction of the moisture detection system and some malfunction of the auxiliary coolant system. (Full description of the assumed accident events are given in Sect. 2.) These two assumed events yield the highest strength loss estimates, ranging from 1.2 to 1.6% for Case 3, and 2.4 to 1.9% for Case 3A.

Accident Cases 4 to 6A assume a design basis depressurization accident (DBDA) occurs concomitant with failure of a steam generator tube. It may be noted, perhaps unexpectedly, that strength loss estimates for these depressurization cases fall below the estimates for nondepressurization of Cases 3 and 3A despite the generally higher temperatures experienced. The reasons for this result are that the depressurization blowdown serves to reduce the oxidant partial pressure, and according to the strength loss model used, graphite corrosion at higher temperatures has a smaller effect than an equal degree of corrosion at a lower temperature.

Since Part I of this study<sup>1</sup> concluded that localized temperature excesses above the nominal play a significant role in determining graphite corrosion rates, a similar effort was made here (outlined in Sect. 5.2.1) to assess the effect of hot spots in the generation of localized zones of high corrosion. Based on a preliminary hot-spot analysis, it was concluded that a temperature excess of 116°C could exist beneath the high radial power factor zone at the time of reactor trip with reasonably high probability. As expected, localized strength losses significantly exceed the nominal values given in Table 1.1. For accident Case 1, the resulting localized strength loss is estimated to be approximately 0.2%, as compared with the cited nominal range of 0.042 to 0.007%. (See Table 5.6 for complete results.) The maximum localized strength loss for the initial 116°C temperature excess occurs for accident Case 3A, where localized zones of 6.8 to 12% strength loss are predicted beneath the high power factor zone.

There exists a smaller probability for higher hot streak temperatures during load following transients. If a steam generator tube were to fail during a rise to power requiring large reactivity insertion for xenon override, a column hot streak 317°C above the coolant average could exist beneath the high radial power zone. The localized strength loss thereby

incurred would be from 1 to 1.5% for accident Case 1, and a maximum range of from 25 to 33% for accident Case 3A.

## 2. DESCRIPTIONS AND TEMPERATURE HISTORIES OF POSTULATED ACCIDENT EVENTS

### 2.1 Description of Postulated Tube Rupture Events

The sequence of eight steam-generator tube rupture scenarios listed below were assumed for this study. These may be separated into two groups: Cases 1 to 3A do not involve depressurization, whereas depressurization due to design basis failure of the prestressed concrete reactor vessel (PCRV) and tube failure are assumed to occur simultaneously in Cases 4 to 6A.

- Case 1. Normal scram following high-moisture detection in one of the six primary coolant loops; successful isolation of the faulty loop and cooldown on the remaining five loops.
- Case 2. Scram following high-moisture detection. Failure to isolate leaking module causes loss of main loop cooling (LOMILC). Cooldown affected by all three core-auxiliary coolant system (CACS) loops after a 5-min startup delay.
- Case 3. Same as Case 2 except that one CACS loop fails to start.
- Case 3A. Power level is assumed to be set at 73.5% with one of the three CACS loops known to be nonfunctional. Cooldown following a scram on one CACS loop after a 5-min startup delay.
- Case 4. Simultaneous tube-burst and design basis depressurization accident (DBDA) scrams reactor. Cooldown affected on five of six main coolant loops.
- Case 5. Simultaneous tube-burst and DBDA scrams reactor. Failure to isolate leaking loop causes LOMILC. Cooldown affected by the three CACS loops after a 5-min startup delay.
- Case 6. Same as Case 5 except that one CACS loop fails to start.

Case 6A. Same as Case 5, but initial power level is assumed to be 73.5% with one CACS loop known to be nonfunctional. Cooldown affected on one CACS loop after 5-min startup delay.

## 2.2 Temperature Transients During Postulated Accidents Calculated by ORECA-3

In order to assess the damage to the core posts as a result of each postulated accident event, it is necessary to know both the coolant temperature environment around the core posts and the coolant impurity compositions during these events.

In this study, the temperature environment of the core post beneath each refueling zone is assumed to be governed by the coolant exit temperature from that zone. These temperatures have been calculated for each of the eight postulated accident conditions using the ORECA-3 code, which is a 3,000 MW(t) version of ORECA-1<sup>3</sup> developed to model the Fort St. Vrain reactor. The ORECA codes were developed at ORNL for the Nuclear Regulatory Commission, and are similar in general purpose and philosophy to the RECA code of General Atomic Company (GAC). A major limitation of the ORECA code is its dependence on external sources for coolant flowrate and mean core inlet temperature history following the scram. These requisite input data were obtained for Case 1 via informal communication from GAC. For Case 3, shutdown flows and the core inlet temperatures were obtained from the GAC response to question 12 regarding LTR-1.<sup>3</sup> The same temperature history was assumed to hold for Cases 2 and 3A and shutdown flowrates were assumed to be 3/2 and 1/2, respectively, times the value given for Case 3. This seemed appropriate since three, two, and one CACS loops are operative for Cases 2, 3, and 3A, respectively.

The temperature and flowrate data given in Fig. 4.26 of LTR-1<sup>5</sup> apply to Case 4 and were assumed for the ORECA calculations. Inlet temperatures and flowrate for Case 6 were obtained from GAC, and are summarized in ref. 4. The core inlet temperature histories were assumed to be the same for Cases 5 and 6A, and the flowrates for these two cases were again assumed to be 3/2 and 1/2 times that of Case 6, simply reflecting the number of CACS loops operative for each case.

The initial reactor power level was assumed to be 105% of that rated for each case, except Cases 3A and 6A, where the initial power levels were set at 73.5%. The newer, so-called "120/110% afterheat curves" were used,<sup>4,6</sup> which assume afterheat production rates 20% above predictions during the first 1000 sec following the scram, and 10% higher thereafter.

Examination of some preliminary ORECA calculations indicated that, as anticipated, temperatures beneath zone 9 (the highest radial power factor zone)\* achieved the highest levels, which indicated that the core posts supporting zone 9 would be most seriously affected by a tube-burst event. In addition to zone 9, zones 11 and 67 were selected for study, the first as being representative of core post conditions beneath a fuel zone with average radial power factor, and the second as being representative of a peripheral zone. The preliminary calculations indicated that peripheral zones, like zone 67, would, in some cases, exhibit temperature excursions of longer duration, but of a less severe degree.

A typical ORECA plot of coolant temperature histories beneath zones 9 and 11 are shown in Fig. 2.1 for the Case 5 event. In addition to graphs like Fig. 2.1, ORECA tabulates coolant temperatures at the core exit for each fuel zone at from 10 to 30 min intervals following the initiating event. A summary of these computer calculations pertaining to refueling zones 9, 11, and 67 for each of the eight postulated accident events is given in Table 2.1.

Core temperature histories during each postulated event are required for the estimation of the impurity compositions to which the core posts are exposed. Since the exposed surface of the core is many times greater than the core posts and also becomes hotter after the scram, the composition of impurities in the primary coolant is controlled by steam reaction with the core graphite. Core temperatures at ten axial locations in each refueling zone were calculated using ORECA for each assumed accident sequence. An example of the ORECA output for the Case 5 accident in zone 9 is illustrated in Fig. 2.2. For this case, the temperature peak is reached in 60 min, and the maximum temperature falls to about 400°C after 300 min.

---

\*For the locations of numbered refueling zones in the core refer to Fig. 4.2-1 of ref. 2.

ORNL DWG 76-679

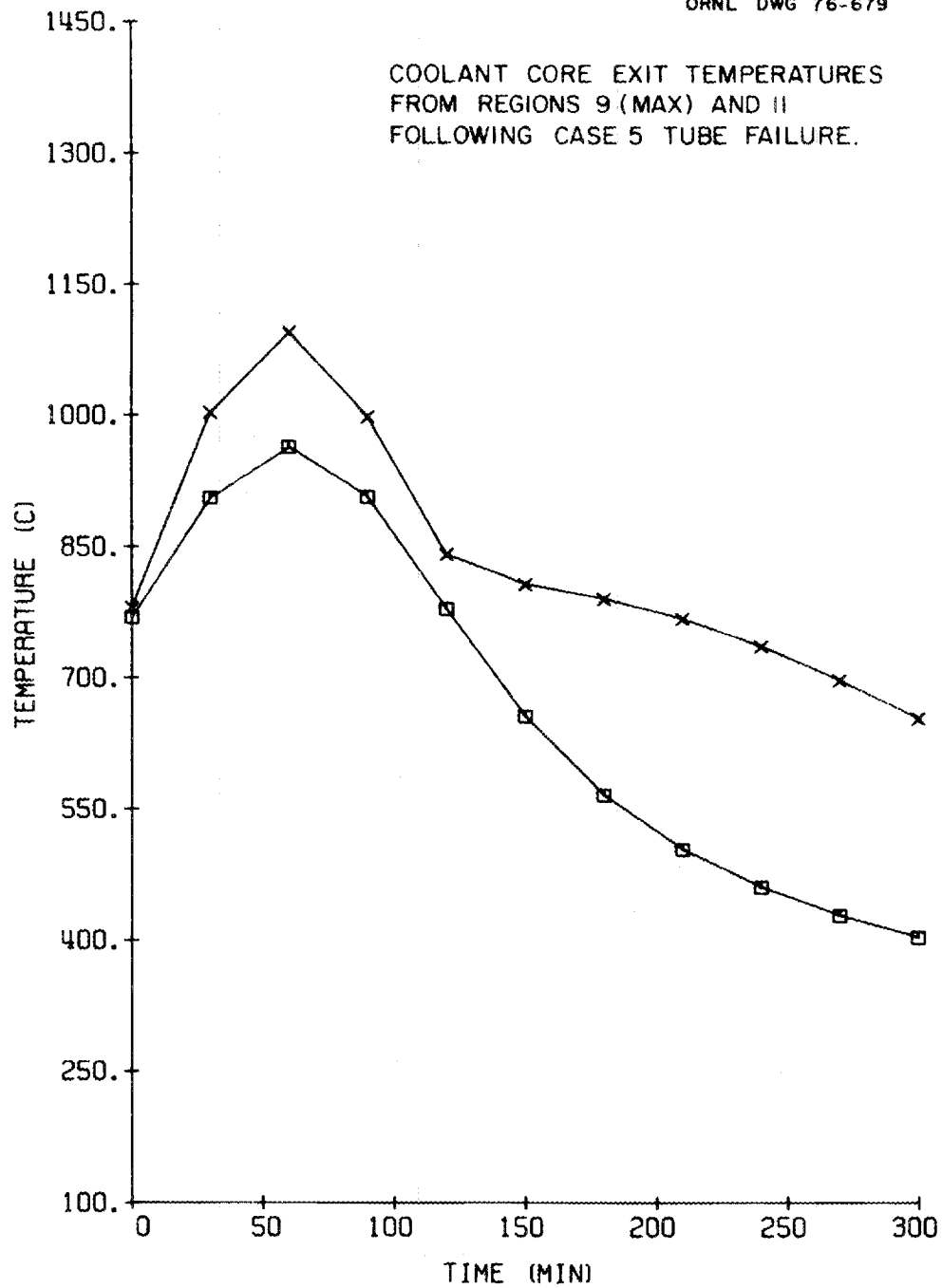


Fig. 2.1. Coolant core exit temperatures from regions 9 (maximum temperature) and 11 following Case 5 tube failure.

Table 2.1. Coolant exit temperatures (°C) from the core at zones 9, 11, and 67 eight tube burst scenarios; calculated using ORECA

Time (min)	Case 1			Case 2			Case 3			Case 3A			Case 4			Case 5			Case 6			Case 6A			
	Zones:			Zones:			Zones:			Zones:			Zones:			Zones:			Zones:			Zones:			
	9	11	67	9	11	67	9	11	67	9	11	67	9	11	67	9	11	67	9	11	67	9	11	67	
0	780	780	780	780	780	780	780	780	780	780	780	780	780	780	780	780	780	780	780	780	780	780	780	780	780
10	340	386	688	794	787	783	838	810	785	830	810	782	748	761	777	854	824	784	842	818	783	809	798	780	780
20	283	301	547	808	794	786	895	840	790	880	839	785	577	632	764	928	869	789	904	856	787	838	815	781	781
30	300	306	546	822	801	790	953	870	795	930	869	788	479	543	752	1002	914	793	967	894	791	867	832	782	782
40	329	321	538	691	694	780	872	811	793	934	875	789	408	466	738	1033	935	797	1025	923	795	900	854	734	734
60				431	481	760	709	695	790	944	887	792	316	338	687	1095	978	804	1142	1012	803	964	897	787	787
90				315	331	643	391	431	744	637	682	788				997	921	810	1229	1104	813	1064	965	792	792
120						458		303	620	355	422	763				809	785	811	1296	1117	822	1164	1036	799	799
150						383			492		321	722				652	650	805	1206	1036	828	1254	1104	805	805
180												667				554	528	790	1056	905	829	1317	1156	811	811
210												603				495	483	767	903	776	823	1339	1177	818	818
240												536				458	438	736	776	694	811	1309	1159	823	823
270												473				431	407	697	677	601	792	1235	1103	828	828
300												438				415	391	668	626	566	776	1167	1049	820	820

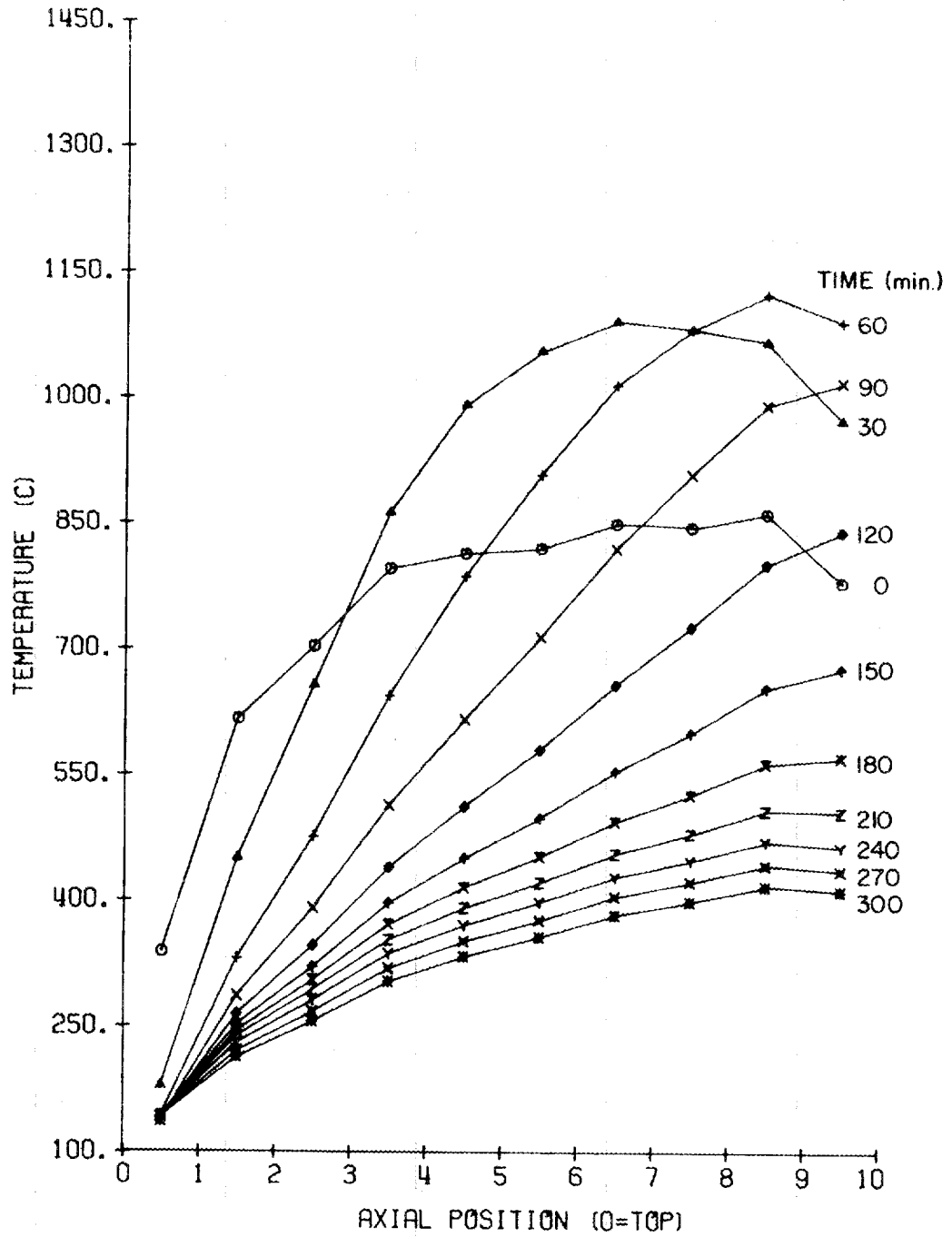


Fig. 2.2. Core temperatures in region 9 following Case 5 tube failure. Calculated using ORECA.

Graphite temperature distributions for each of the 85 fuel zones were used to compute the "reaction-average" temperature history of the core for each of the eight assumed events. The rationale and derivation for reaction-averaging is given in ref. 1; briefly, the motive is to characterize the core with a weighted-average temperature which properly accounts for the strong temperature dependency of the steam-graphite reaction. The simple, space-average does not sufficiently emphasize the importance of the higher temperature areas.

It can be shown<sup>1</sup> that for a reaction rate with a typical activation energy temperature dependency, an appropriate weighted average temperature may be computed from

$$T_{ra} = \frac{-\Delta H/R}{\ln \left[ \frac{\sum_i^N \frac{A_i}{A_T} \exp \left( -\frac{\Delta H}{RT_i} \right)}{\sum_i^N \frac{A_i}{A_T}} \right]} \quad (2.1)$$

where

$\Delta H$  = activation energy for the corrosion reaction, assumed to be 50 kcal/mol,

$R$  = gas constant,

$A_i$  = area of the  $i$ -th core region, which experiences a uniform temperature,  $T_i$ ,

$N$  = total number of regions = 10 x 73,

$A_T$  = total core surface area.

Reaction-averaging of the core temperature was incorporated in the ORECA code and computed following each case run. A summary of these results are shown in Fig. 2.3, where the dashed lines refer to the four non-DBDA cases and the solid lines represent core average temperatures for the four cases involving primary circuit depressurization. These appropriately weighted core temperatures were employed as input for the  $\phi$ XIDO program where they were used to determine the coolant impurity composition. Whenever a reaction rate is known to vary with temperature with the usual activation-energy dependency, the reaction-average technique is a simple alternative to subdividing the core into smaller, uniform temperature zones in order to find the overall reaction rate throughout a variable temperature region.

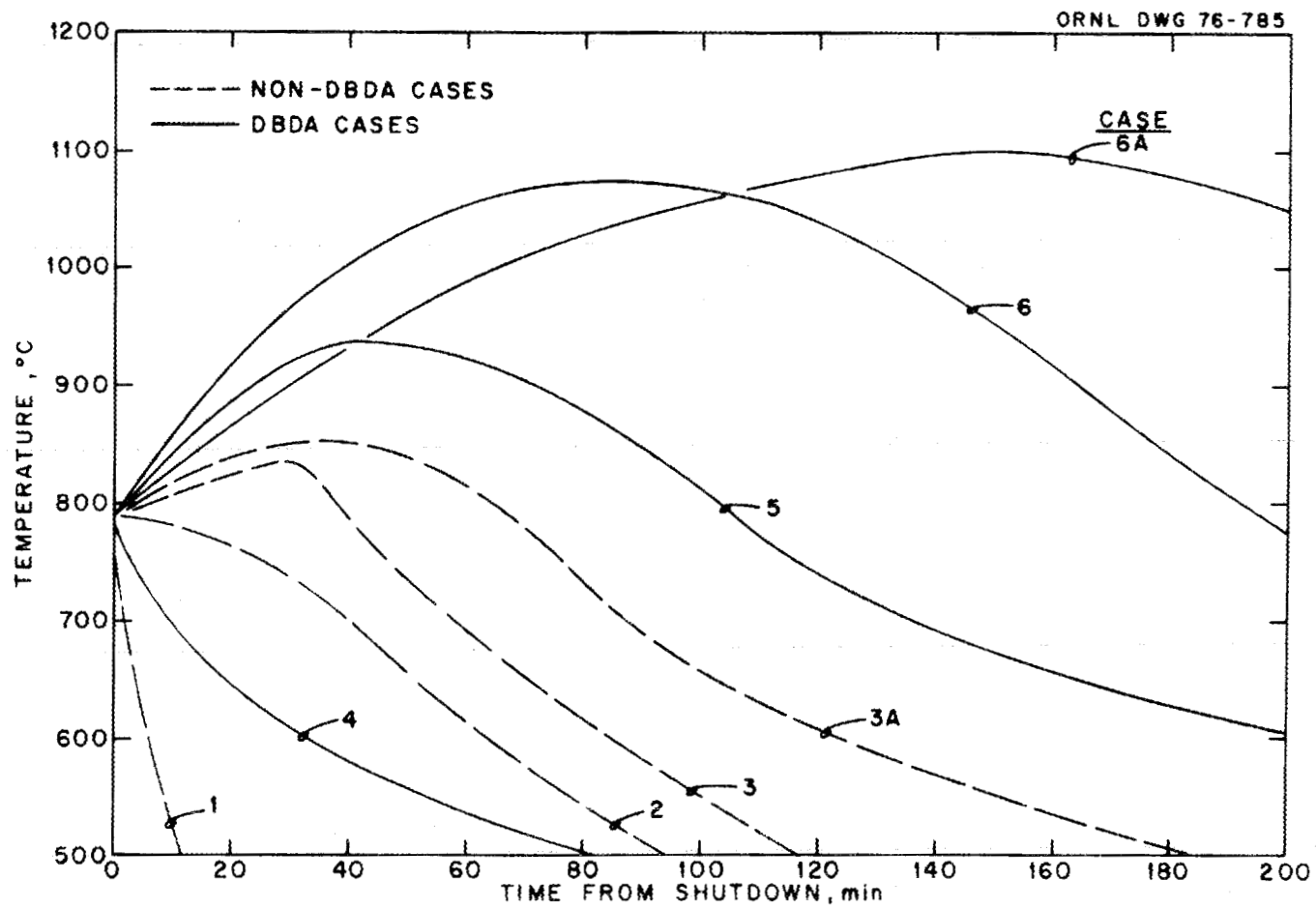


Fig. 2.3. Reaction-average HTGR core temperature following postulated accidents.

Figure 2.4 shows a comparison for Case 5 between the maximum temperature (exhibited in region 9), the calculated "reaction-average" core temperature using Eq. (2.1), and the flat, area-average core temperatures. As anticipated, the reaction-average temperature is in general higher than the area-average (by approximately 100°C) reflecting the greater importance of the higher temperature regions in fixing the overall core reactivity to steam corrosion.

### 2.3 Assumed Moisture Ingress Rates Following Tube Failure

If the moisture monitoring system (MMS) functions is intended, as it is assumed in Cases 1 and 4, the leaking steam generator is isolated and the dump of its contents is initiated approximately 93 sec after the tube-failure event. Barsell<sup>7</sup> gives the following idealized schedule of ingress rates for such a case:

1. 0 to 3 sec. The moisture ingress rate drops linearly from an initial value of 22.7 kg/sec (50 lb<sub>m</sub>/sec) to 10.9 kg/sec (24 lb<sub>m</sub>/sec).
2. 3 to 92 sec. The moisture ingress rate remains steady at 10.9 kg/sec.
3. 92 to 122 sec. In this 30-sec interval following isolation and dump, the leakage rate drops linearly to zero from 10.9 kg/sec.

Thus the total ingress is 1180 kg (2607 lb<sub>m</sub>) for such cases, and it extends over an approximate 2-min period. Program ~~OX~~OXIDO, used in this study, further idealizes the estimated ingress rate by completely leveling it for the initial 2-min period. Thus, a steady ingress rate of 548 mol/sec over the initial 2-min period is assumed for Cases 1 and 4, which yields an equivalent total ingress to that indicated above. The effect of leveling the ingress rate over a 2-min period on the computed results is expected to be miniscule.

If the MMS fails to identify the leaking steam generator, as is assumed for all cases except 1 and 4, present plans would allow the

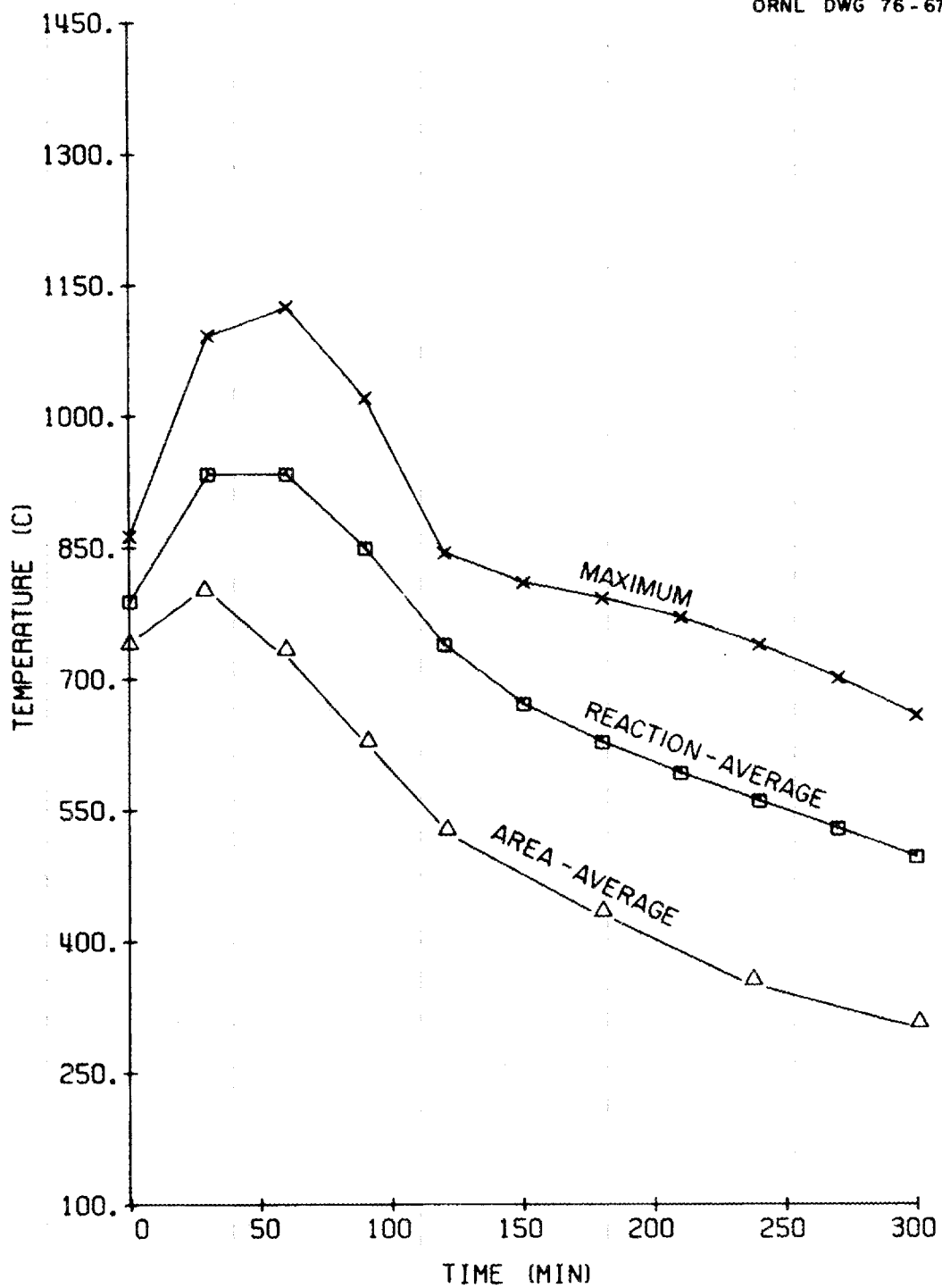


Fig. 2.4. Maximum, reaction-average, and area-average core temperatures following Case 5 tube failure.

operator to manually dump up to two (of the six) primary loops. In the event that the faulted steam generator is missed, it will continue to leak until pressures are equalized between the steam generator and the primary system. However, during this interval, check valves on the feedwater and superheated lines extending from the steam generator would preclude leakage from the other five loops back through the failed tube.

Little information has been found on projected moisture ingress rates for cases where the MMS fails to identify the faulted loop. In this study, it has therefore been assumed that the entire contents of the failed steam generator leak to the primary system in cases where it is not identified and dumped.

No published values have been located on estimated water inventories in 3000 MW(t) HTGR steam generators; and, indeed, the steam generator design is evidently being revised at the time of this writing. For the purpose of this study, these inventories were estimated in the following way: (1) present estimates for the sizes and lengths of the feedwater, economizer, evaporator and superheated portions of the steam generator were obtained by informal communication;<sup>8</sup> and (2) it was assumed that the feedwater and economizer sections were completely full of water, and the evaporator section contained water in one-half of its volume. The mass of steam in the evaporator and superheater were neglected.

This leads to an estimated inventory of water in the steam generator of 6090 kg. In this study, it was assumed that for the MMS failure cases this estimated water inventory is discharged into the primary system at a steady rate over the initial 10-min period following tube failure. This is equivalent to an assumed ingress rate of 563 mol/sec or 22 lb<sub>m</sub>/sec for the initial 10-min period.

### 3. GRAPHITE CORROSION RATES DURING STEAM GENERATOR TUBE RUPTURE EVENTS

There is some difficulty in the proper estimation of corrosion rates of both core and support post graphite during a tube burst event in that the majority of published kinetics correlations are based on data taken with steam partial pressures substantially below anticipated levels. For

example, the maximum steam partial pressure for the six published studies reviewed in ref. 1 is 0.01 atm, and the most extensive study, that of Wicke et al.,<sup>9</sup> which is the basis for the correlation used in the OXIDE-3 program,<sup>7</sup> utilized a maximum steam pressure of only 0.001 atm. On the other hand, calculations presented in Sect. 5 will show that steam levels for the events studied peak at from 1.5 to 12 atm. The published corrosion equations are essentially empirical equations from 2 to 6 constants, and as such should properly be used only within the range of the stated experimental conditions. Extrapolation of such empirical formulae over the large range indicated between experimental and projected steam partial pressure could yield significant error in estimated corrosion rate.

Hence, the literature was scanned for graphite corrosion rate information at conditions closer to those anticipated during tube burst events. Three such studies, which are reviewed briefly in the following section, were sufficiently complete to allow formulation of a corrosion rate expression.

### 3.1 Steam Corrosion of Experimental Gas-Cooled Reactor (EGCR)

#### Graphite by Helms and MacPherson

Helms and MacPherson<sup>10</sup> (designated HM below and in the figures) measured the corrosion rate of full-scale segments of both EGCR fuel element graphite, Speer 901-RYL, and EGCR moderator graphite (manufactured by the National Carbon Company) by pure, superheated steam. The experimental facility used for these tests is shown diagrammatically in Fig. 3.1. The specimen, which was approximately 74 cm long x 12.7 cm diam x 2.54 cm thick, was exposed at the internal surface to the superheated steam. Thermocouples embedded in the graphite recorded the specimen temperature, and analysis of the off-gas by a chromatograph was used to follow the degree of corrosion.

Two types of test series were performed for each material. First, the graphite temperature was held constant at 760°C while the steam pressure was varied from 3.0 to 21 atm. This was followed by a series of runs on fresh material at temperatures ranging from 730 to 870°C with constant steam pressure of 11 atm, to burnoffs of up to 50%. From these runs it

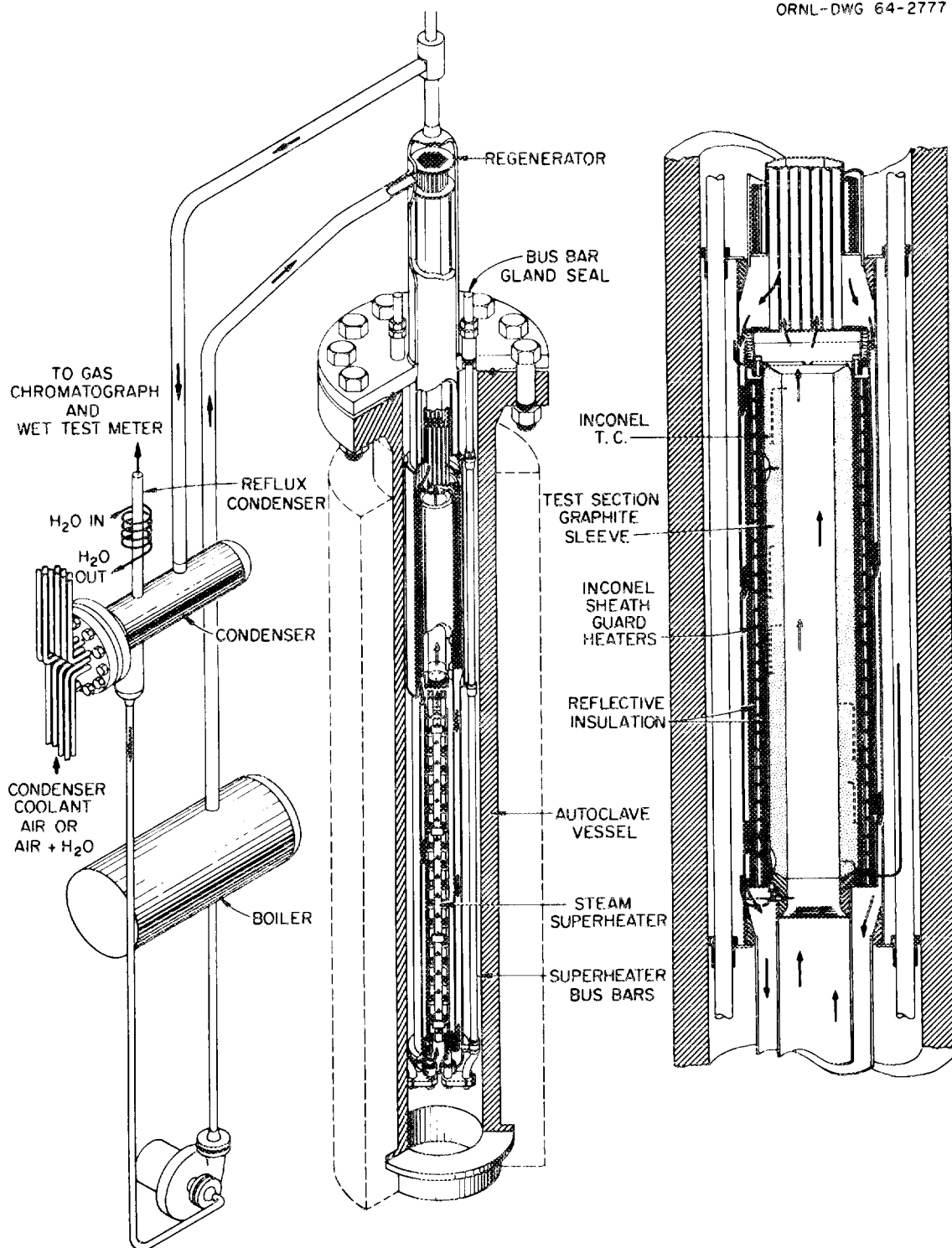


Fig. 3.1. Steam-graphite experimental facility of Helms and MacPherson.<sup>10</sup>

was possible to discern the effects of steam pressure, burnoff, and temperature on the corrosion rate. The results for EGCR moderator graphite were correlated by the following empirical equation valid for a burnoff range of from 0.5 to 50%.

$$R'_s = 1.07 \times 10^{11} B^{0.150} \exp(-52,200/RT), \quad (3.1)$$

where

$$R'_s = \text{corrosion rate, mg carbon hr}^{-1} \text{ cm}^{-2},$$

$$B = \text{burnoff, percent.}$$

Results for Speer fuel element graphite were very similar at low burnoffs, but the rate increased with level of burnoff somewhat more rapidly than is indicated by Eq. (3.1).

As the correlation equation implies, steam pressure variation did not significantly affect the observed corrosion rate throughout the range of the experimental conditions. The indicated activation energy of 52,200 cal/mol falls directly in the range observed for other similar experiments. The nature of the experiment did not allow estimation of inhibition effects due to CO and H<sub>2</sub>, but these must have been relatively minor, because no axial corrosion gradient was apparent for the rather lengthy specimens (i.e., corrosion was observed to occur uniformly at the inner surface with no significant alteration of contour).

### 3.2 Experiments of Johnstone, Chen, and Scott

Corrosion experiments on graphite, identified solely as National Carbon Company graphite, were conducted by Johnstone, Chen, and Scott<sup>11</sup> (designated as JCS) through the temperature range 860 to 940°C and steam partial pressure range 0.55 to 0.95 atm. Hydrogen inhibition was investigated by hydrogen additions to the feed gas to levels of 0.04 to 0.2 atm. All the experiments were conducted at atmospheric pressure with the balance of the feed gas composed of nitrogen.

Physical characterization of the graphite indicated an initial density of 1.65 g/cm<sup>3</sup> corresponding to a total porosity of 26%. The initial BET surface area of 1.15 m<sup>2</sup>/g was found to increase rapidly with burnoff. At 12% burnoff, the observed BET surface was approximately 11.1 m<sup>2</sup>/g.

The graphite specimens were about 1-in.-long annular cylinders, exposed at the inner surface. The specimens were of 3.8 cm diam with 6.4-mm wall thickness. So-called integral experiments were also performed on specimens up to about 1 m in length. The degree of corrosion was calculated by standard chemical analysis of the product gas stream.

Results for the differential experiments are embodied in the following derived equation:

$$R_v = \frac{26.9 \exp(-26,000/RT) P_{H_2O}}{1 + 6.48 \times 10^{-11} \exp(62,200/RT) P_{H_2} + 6.19 \times 10^{-16} \exp(79,700/RT) P_{H_2O}} \quad (3.2)$$

where

$R_v$  = reaction rate, g/g-min,

$P_{H_2O}$ ,  $P_{H_2}$  = partial pressures, atm.

The reaction rate was observed to increase with burnoff more rapidly than found by Helms and MacPherson; for example, the rate increased by a factor of 2.7 between 1 and 5% burnoff at 1000°K,  $P_{H_2O} = 0.5$ , and  $P_{H_2} = 0.1$  atm. An unusual observation was that both the multiplicative constants and activation energies were found to vary with burnoff. Equation (3.2) represents conditions at 1% burnoff.

Since the corrosion depths at these experimental temperatures are anticipated to be about 2 mm (Sect. 4.2, ref. 1) compared with an actual specimen thickness of 6.4 mm, it is necessary to use the so-called large specimen correction to convert Eq. (3.2) to equivalent surface units. This is necessitated because the rate is expressed in terms of sample mass; evidently, only a portion of the mass participated in the reaction. Section 4.1 of ref. 5 describes the means for converting slab geometry as:

$$R_s \left( \frac{\text{mol}}{\text{cm}^2 \cdot \text{min}} \right) = R_{\text{app}} \left( \frac{\text{g}}{\text{g} \cdot \text{min}} \right) \frac{\Delta h \cdot \rho}{M_w}, \quad (3.3)$$

where

$R_{\text{app}}$  = apparent corrosion rate given by Eq. (3.2),

$\Delta h$  = specimen width,  
 $\rho$  = graphite density,  
 $M_w$  = molecular weight of carbon.

Substitution of the appropriate values yields the equivalent of Eq. (3.2) based on exposed surface:

$$R_s \left( \frac{\text{mol}}{\text{cm}^2 \cdot \text{min}} \right) = \frac{2.35 \exp(-26,000/RT) P_{\text{H}_2\text{O}}}{1 + 6.48 \times 10^{-11} \exp(62,000/RT) P_{\text{H}_2} + 6.19 \times 10^{-16} \exp(79,700/RT) P_{\text{H}_2\text{O}}} \quad (3.4)$$

### 3.3 High-Pressure Experiments of Blackwood and McGrory

Experiments most closely approaching the corrosive conditions in the HTGR primary system following tubing rupture were performed by Blackwood and McGrory<sup>12</sup> (designated BM). Unfortunately, the material used was purified coconut charcoal with the ash extracted by use of hydrochloric and hydrofluoric acids. The initial material possessed an internal surface area of about 47 m<sup>2</sup>/g, as compared with a range of 0.1 to 0.5 m<sup>2</sup>/g for reactor grade graphite. Hence, the utility of these experiments is greatly reduced.

The conditions for the Blackwood and McGrory experiments are summarized in Table 3.1. Note that the particle size of the charcoal was about 1.7 mm, which was calculated as the root mean square of the upper and lower mesh sizes used in the sieving procedure. This feature classifies these experiments as "small specimen" tests in that the corrosion should have extended throughout each particle more or less uniformly. A constant space velocity of 2 vol/sec was selected for most runs. This was the maximum flow conveniently attainable in the apparatus, necessitating the use of nitrogen as a diluent in the feed gas in order to achieve the desired range of experimental conditions. At the termination of the test series, it was found that the results were sensitive to flow rate through the apparatus even at this maximum rate. Thus, the reported "kinetics constants" include an unresolved component due to mass transport.

Table 3.1. Conditions for the experiments of Blackwood and McGrory<sup>12</sup>


---

Temperatures, °C	750, 790, 830
Pressure of feed gas, atm	
Total pressure	1 → 50
H <sub>2</sub> O partial pressure	1 → 50
H <sub>2</sub> partial pressure	0 → 3
N <sub>2</sub> partial pressure	Used as diluent to maintain a space velocity of 2 vol/sec.
Charcoal composition (%)	
Hydrogen	0.44
Oxygen	1.67
Nitrogen	0.19
Ash	0.13
Iron	0.001
Halides	0.001
BET surface, m <sup>2</sup> /g	46.5
Bulk density	0.5
Particle size, British standard sieve	-7 + 14 (rms size = 1.7 mm)

---

Some of the main conclusions presented by Blackwood and McGrory based on their data are the following:

1. At 830°C and low  $P_{H_2}$ , a corrosion rate "practically linear" with  $P_{H_2O}$  was observed.
2. An order of reaction greater than unity with respect to steam was found at higher  $P_{H_2}$  and lower temperature.
3. Methane production was found to be directly proportional to the steam partial pressure and independent of the hydrogen partial pressure. Since H<sub>2</sub> depressed the primary corrosion reaction, the proportion of CH<sub>4</sub> produced in the off-gas increased with increasing  $P_{H_2}$ .

An essentially curve-fitting procedure yielded the following form of correlation for the experimental data:

$$R_v = \frac{k_1 P_{H_2O} + k_4 P_{H_2} P_{H_2O} + k_5 P_{H_2O}^2}{1 + k_2 P_{H_2} + k_3 P_{H_2O}}, \quad (3.5)$$

where  $R_v$  is in units of mol/g·min, and the partial pressures are exposed as atmospheres. The reported values for the constants at the three test temperatures are given in Table 3.2.

Table 3.2. Constants for Blackwood and McGrory corrosion rate equation<sup>a</sup>

Temperature (°C)	$k_1$	$k_2$	$k_3$	$k_4$	$k_5$
750	$0.36 \times 10^{-4}$	35	0.06	$0.3 \times 10^{-4}$	$1.5 \times 10^{-6}$
790	$1.25 \times 10^{-4}$	35	0.09	$0.5 \times 10^{-4}$	$1.5 \times 10^{-6}$
830	$3.7 \times 10^{-4}$	35	0.14	$1.05 \times 10^{-4}$	$1.5 \times 10^{-6}$

<sup>a</sup>Constants for Eq. (3.5); units will yield corrosion rate as mol/g·min, with pressure in atmospheres.

Although the Blackwood and McGrory experiments are interesting because of the large ranges of reactant pressures employed, this correlation was not utilized for the calculation of core post corrosion rates due to a number of uncertainties. The use of charcoal instead of graphite, and the unresolved effect of reactor space velocity coupled with a rather narrow temperature range, rendered the use of a five-constant empirical equation to be subject to possibly excessive error. Nevertheless, the correlation was compared with the others examined in the next section.

#### 3.4 Comparison of Corrosion Rate Expressions in the High Steam Pressure Regime

The three empirical corrosion rate expressions presented in Sects. 3.1-3.3 are compared on a uniform basis, namely, the predicted rate based on the exposed surface area of a large specimen. The Helms and MacPherson expression, Eq. (3.1), already appears in this form. The Johnstone, Chen, and Scott<sup>11</sup> expression was converted to this basis in Sect. 3.2, and is

given by Eq. (3.3). The method for converting a small specimen expression, given in terms of moles per gram of sample per unit of time [e.g., Eq. (3.5) for the Blackwood and McGrory work] has been presented in Sect. 4.2-1 of ref. 7 where the procedure was used to convert the results of a similar type of experiment to surface units. It shows that the appropriate conversion to surface units is given by

$$R_V \left( \frac{\text{mol}}{\text{g} \cdot \text{min}} \right) \cdot \rho \Delta h = R_S \left( \frac{\text{mol}}{\text{cm}^2 \cdot \text{min}} \right) \quad (3.6)$$

where

$\rho$  = graphite density,

$\Delta h$  = active corrosion depth of a large specimen.

Equation (3.6) simply states that the observed corrosion rate per unit area of a large specimen equals the rate observed per unit mass of a uniformly corroding small specimen, multiplied by the mass of graphite per unit area being corroded. A problem in this conversion is that the active corrosion depth,  $\Delta h$ , varies with temperature (diminishing with increasing temperature), and the conversion to surface units thus is temperature dependent. The variation is modest compared with other possible sources of error, and selecting a value for  $\Delta h$  corresponding to some representative temperature is adequate in this case. At 800°C, a corrosion depth of 0.26 cm is indicated,<sup>1</sup> yielding a value of 0.44 for the product,  $\rho \Delta h$ , in Eq. (3.6).

The three above-mentioned expressions are compared in Fig. 3.2 assuming a steam of hydrogen pressure of 10 and 1 atm respectively, as a function of a temperature between about 730 and 1030°C. The Helms and MacPherson expression is independent of the assumed values for the partial pressures. Figure 3.2 shows fairly good agreement between the HM and JCS expressions above about 800°C for the selected pressure levels.

Figure 3.3 illustrates the predicted variation with steam partial pressure in the high-pressure range, at 1200°K and at both  $P_{\text{H}_2} = 0$  and 1 atm. The HM correlation, which is zero-order with steam pressure throughout its entire range, is flat. JCS at zero hydrogen pressure in the feed gas does not become relatively zero order until about 15 atm of steam pressure; addition of hydrogen to the feed both slows the corrosion rate and causes the sensitivity to  $P_{\text{H}_2\text{O}}$  to be retained to higher pressures.

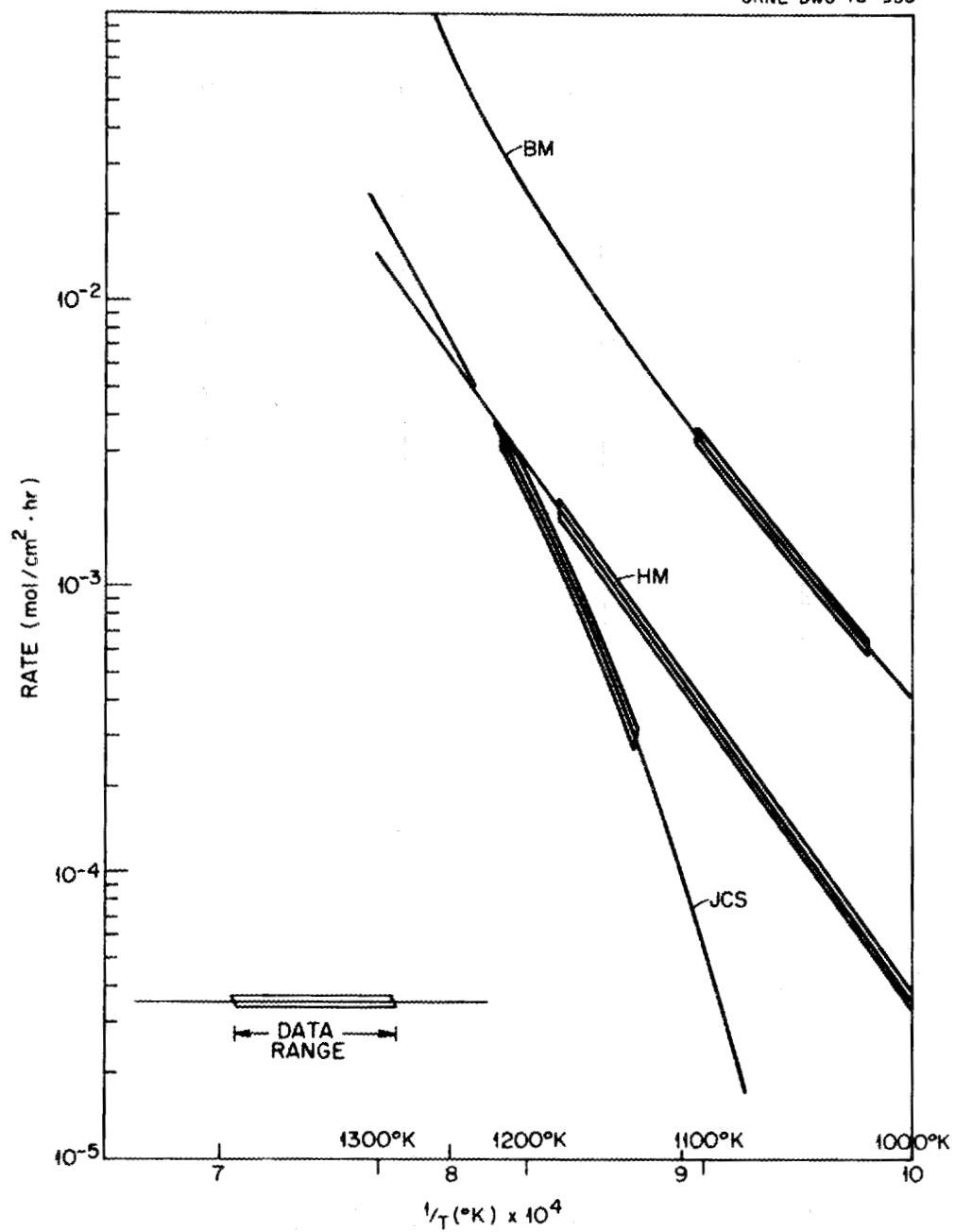


Fig. 3.2. Comparison of predicted corrosion rates at  $P_{\text{H}_2\text{O}} = 10 \text{ atm}$ ,  $P_{\text{H}_2} = 1 \text{ atm}$ . (HM correlation independent of pressure.)

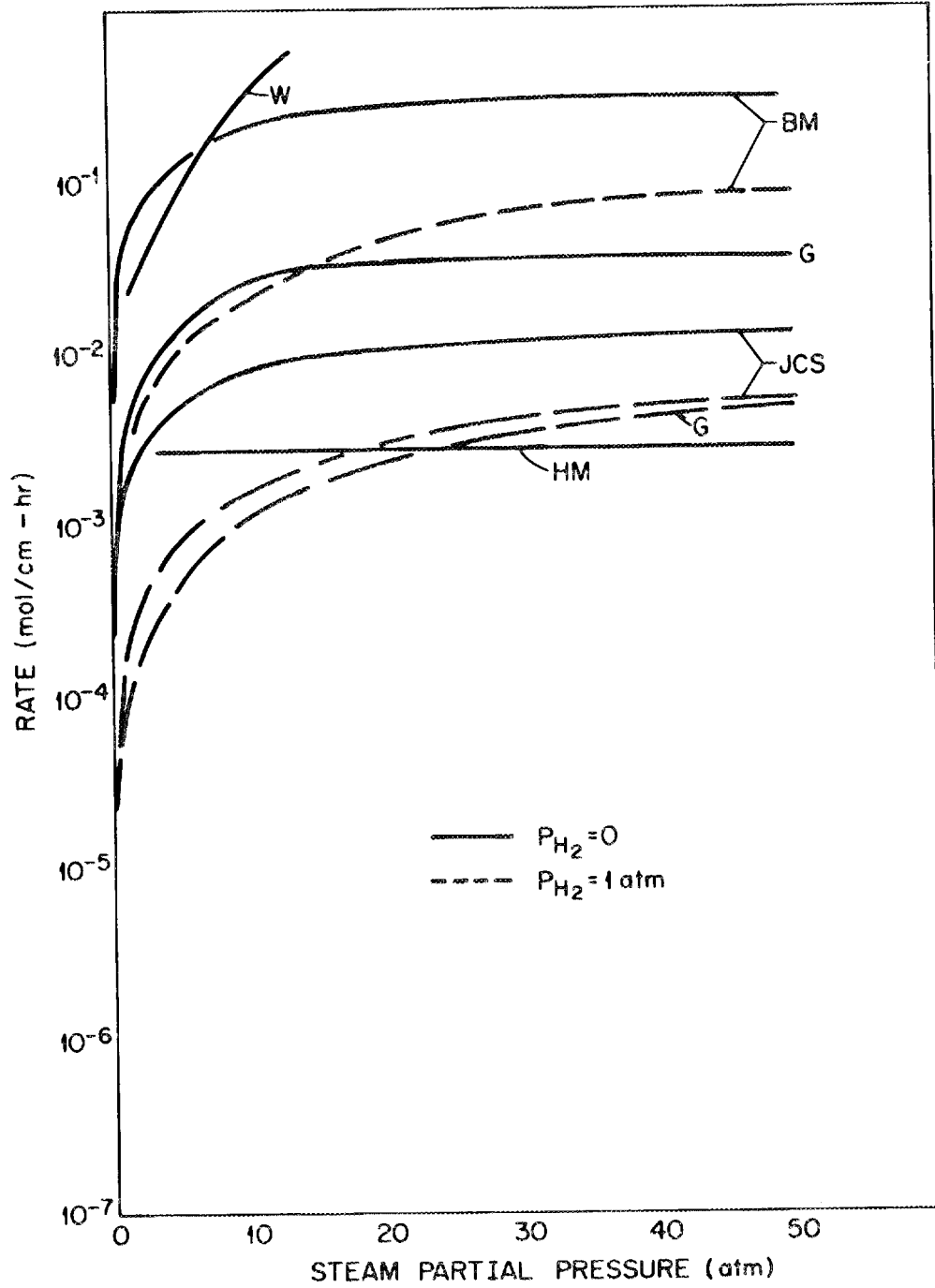


Fig. 3.3. Comparison of graphite corrosion rate expressions at high-steam pressure, 1200°K.

Similar behavior is illustrated by the BM expression except at a correspondingly higher predicted corrosion rate; that is, at zero  $P_{H_2}$  the rate is essentially zero order above about 10 atm of steam pressure, and addition of  $H_2$  both depresses the rate and causes a retention of sensitivity to  $P_{H_2O}$  at higher pressures.

Again, there is a relatively good agreement between JCS and HM above 1 atm. As may have been anticipated, BM yields higher predicted rates in view of the more reactive material used in those tests.

For comparison, two low-pressure kinetics expressions are plotted in Fig. 3.3 to high-steam partial pressures. The Wicke expression [Eq. (15), ref. 1] labeled W in the figure, shows the steepest dependence on  $P_{H_2O}$  at high pressure. This is as anticipated since the highest value of steam pressure used was 0.001 atm, and no steam pressure inhibition term is used in the correlation. On the other hand, the Giberson equation [labeled G in Fig. 3.3 and given as Eq. (18) of ref. 1] does have a steam pressure inhibition term, and it shows a reasonable comparison with HM and JCS despite being based on test data no higher than 0.01 atm  $H_2O$ .

Figure 3.4 illustrates the degree of  $H_2$  inhibition at 1200°K and an assumed steam pressure of 10 atm. The two "high pressure" expressions, BM and JCS, show approximately parallel behavior, while the two low-pressure expressions, G and W, illustrate an extremely steep inhibiting effect at low hydrogen pressure.

### 3.5 Selection of Corrosion Rate Expressions Used in This Study

As a result of the comparisons of steam-graphite corrosion experiments outlined in Sects. 3.1 to 3.4, a judgment was made to utilize both the Helms and MacPherson,<sup>10</sup> and the Johnstone, Chen, and Scott<sup>11</sup> studies as a basis for estimating core and support post corrosion during a tube-burst event. Both of these studies were sufficiently complete to enable development of a corrosion rate equation, which is a requisite for any systems study and is also necessary for extrapolation to anticipated primary loop conditions. Since the Helms and MacPherson study was conducted using pure steam, it is expected to yield lower estimates of the corrosion rate for any particular

ORNL DWG 76-934

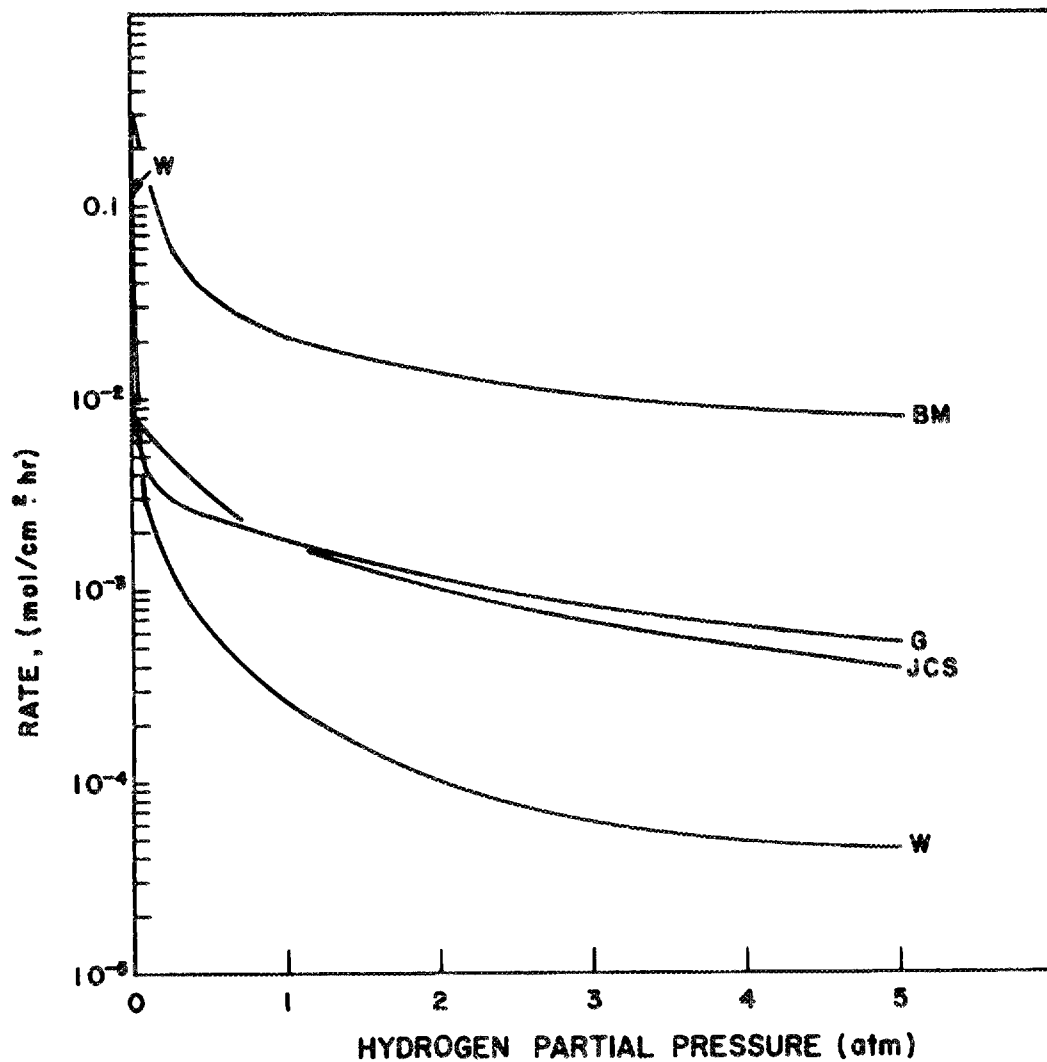


Fig. 3.4. Predicted inhibiting effect of hydrogen at steam partial pressure = 10 atm,  $T = 1200^{\circ}\text{K}$ .

set of conditions. On the other hand, the Johnstone, Chen, and Scott study should yield higher estimates because it is based on 1 atm experiments with steam pressures not exceeding 0.95 atm.

The HM and JCS expressions should bracket the anticipated range of corrosion rates. However, the predicted core post strength loss is somewhat buffered against errors in predicted corrosion rate. For example, an error on the low side in predicting the corrosion rate for the core graphite yields, as a result, a correspondingly more aggressively oxidizing atmosphere in the primary system, and hence tends to increase the predicted rate for the support posts. Conversely, use of an expression that overpredicts the rate would yield a more mild atmosphere and, hence, would tend to underpredict support post corrosion rates.

#### 4. METHOD OF CALCULATION. ØXIDO PROGRAM

##### 4.1 ØXIDO Program Description

The general features of the ØXIDO program used for this study are illustrated in Fig. 4.1. As the figure denotes, each case requires as input the temperature history of the core posts and the reaction-average temperature history of the core graphite. The latter is needed for the calculation of the coolant composition as a function time following the tube rupture, since the coolant composition is overwhelmingly determined by the reaction of steam with the hotter and more massive core graphite. The temperature histories were calculated using the ORECA code as indicated in Sect. 2.

The input parameters also select the type of accident event from one of the eight postulated cases described in Sect. 2.1. This selection fixes the steam ingress rate (Sect. 2.3) and whether depressurization occurs in the selected accident sequence.

In the depressurization cases 4, 5, 6, and 6A, the total pressure is assumed to fall at a rate that is proportional to primary system pressure excess over 1 atm; that is,

ORNL DWG 76-1047

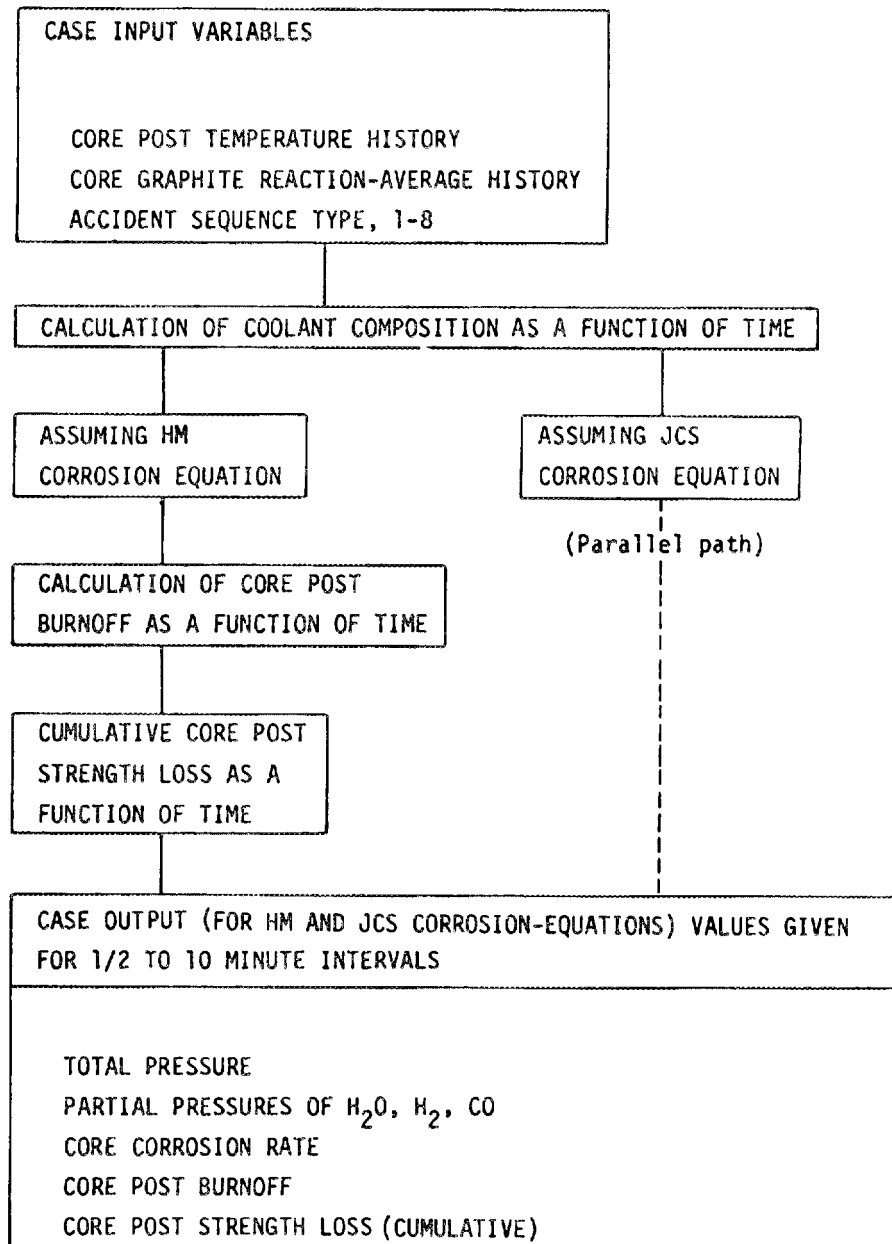


Fig. 4.1. General outline of the OXIDO Program.

$$\frac{dP_T}{dt} = C (P_T - 1) , \quad (4.1)$$

where  $P_T$  is the total pressure of the primary coolant in atmospheres. The value of the proportionality constant,  $C$ , of  $2 \times 10^6 \text{ cm}^3/\text{sec}\cdot\text{atm}$  was selected to yield approximately 95% complete depressurization in 3 min. Calculations employing OXIDE-3 and a 100-in.<sup>2</sup> breach of the PCRV (ref. 7, pp. 4-56) indicate the depressurization to be virtually complete in approximately 2 min under these conditions. This factor is not critical for core post burnoff determinations, and whether the depressurization is completed in 1 or 10 min has no significant effect on the calculated core post strength loss.

Relief valve venting rates for the nonpressurization cases were also computed using Eq. (4.1) with an appropriately smaller value for the proportionality constant,  $C$ . Venting performance was idealized in OXIDO by assuming that only one relief valve exists in the primary circuit (instead of two) which opens at 2 atm overpressure and reseals when the total pressure drops below the original, nominal, primary-loop pressure. It was found that a value of  $1 \times 10^5 \text{ (cm}^3/\text{sec}\cdot\text{atm)}$  for the proportionality constant in Eq. (4.1) yielded approximately the venting behavior reported in ref. 7. Again, no great effort was expended to more accurately model venting behavior in OXIDO, because support post strength loss estimates are not affected much by moderate differences in relief valve characterization.

The coolant composition and total pressure were calculated by a simple forward-stepping procedure indicated by Eqs. (4.2)-(4.4).

$$\frac{d[H_2O]}{dt} = \left( W_s - R_c A_c - Q [H_2O] \right) / V_p \quad (4.2)$$

$$\frac{d[H_2]}{dt} = \left( R_c A_2 - Q [H_2] \right) / V_p \quad (4.3)$$

$$\frac{d[He]}{dt} = Q [He] / V_p \quad (4.4)$$

In the above,  $Q$  may be either the relief valve venting rate or the volumetric blowdown rate during a depressurization event. The brackets,

[ ], denote units of  $\text{mol}/\text{cm}^3$ ;  $W_s$  is the steam ingress rate in  $\text{mol}/\text{sec}$ ;  $R_c$  is the corrosion reaction rate per unit area of core graphite of exposed surface area,  $A_c$ ; and  $V_p$  is the primary system volume. The partial pressure of CO was taken as equal to  $H_2$ , and the total pressure for each time interval was computed from the ideal gas law.

For most of the runs, the calculational time interval was set at 1 sec to minimize accumulated error, and the variable values were stored and outputted at 1 min intervals.

As already noted in Sect. 2.2, core temperatures were characterized by a "reaction-average" temperature, defined by Eq. (2.1). The value of  $R_c$  in Eqs. (4.2) and (4.3) was based on this effective core temperature. This method, which was developed for the TIMOX program described in ref. 1, affords a great simplification over the usual method entailing subdivision of the core into approximately uniform temperature regions and summing rates for each region. The two methods are equivalent when each subdivision is sufficiently small to be characterized by the simple area-average temperature. It was shown that one row of a refueling zone meets this criterion for temperature uniformity within a subdivision; hence, the core reaction-average temperature was computed by ORECA by summation of rows and refueling zones according to the procedure defined by Eq. (2.1).

#### 4.2 Calculation of Core Post Burnoff and Strength Loss

Support post burnoffs were computed for each time interval by using the appropriate input temperature for the selected accident sequence and refueling zone. These temperatures were taken to be equal to the exit coolant temperature from the core beneath the refueling zone, as predicted by the ORECA code.

The post beneath refueling zones 9, 11, and 67 were selected for study. Zone 9 reflects the case of the highest radial power factor zone, where the support posts exhibit highest temperatures during tube burst events. Zone 11 portrays conditions under the average zone, and zone 67 was taken as a typical peripheral zone. One such peripheral zone was selected for study because the calculated temperature histories indicated

that while these locations did not achieve temperatures as high as the more interior zones, the duration of the temperature excursion was longer.

OXIDO calculates the post burnoffs using both the Helms and MacPherson (Eq. 3.1) and the Johnstone, Chen, and Scott (Eq. 3.4) expressions described in Sect. 2. Parallel calculations are made in the program.

The procedure for estimating support post strength loss follows closely that described in ref. 1 for the slow steam ingress study, with the exception that the temperature is variable throughout the time involved, whereas previously it was assumed to be constant. For the case of burnoff at constant temperature it was shown that the fractional strength loss, FSL, of a support post of diameter D, may be represented by

$$FSL = 1 - \left( 1 - \frac{2 P(T) BO}{\rho_{bo} D} \right)^2, \quad (4.5)$$

where  $\rho_{bo}$  is approximately 10% less than the graphite density, and P(T) is a temperature-dependent parameter varying approximately inversely with temperature, as indicated by Eq. (4.6).

$$\left. \begin{aligned} P(T) &= 14, & T < 1000^\circ\text{K} \\ P(T) &= 1 + 6.42 \times 10^{-5} (1200 - T)^2, \\ P(T) &= 1. & T > 1473^\circ\text{K} \end{aligned} \right\} \quad (4.6)$$

Equation (4.5) was also used in OXIDO for calculation of strength loss with the exception that incremental additions to the value of FSL were made using the appropriate temperature and calculated burnoff for each time interval: usually, 1 min. Section 6 of ref. 1 gives a fuller discussion of this basis for estimating support post strength loss.

## 5. CORE POST STRENGTH LOSS ESTIMATES

### 5.1 Strength Loss Estimates for the Nominal Core Post Supporting Zones 9, 11, and 67

The detailed results of the calculations using the OXIDO program for Cases 1, 2, 3, and 3A, the nondepressurization cases defined in Sect. 2.1, are shown in Table 5.1. The left portion of the table pertains to the

Table 5.1. Tabulated results for Cases 1, 2, 3, and 3A (non-DBDA cases) using  $\mu$ XIDO. Strength loss estimates for the nominal core posts

Case	Time (min)	Reaction-ave. core temp (°C)	Steam ingress rate (mol/s)	HM <sup>a</sup>				No. of vents	JCS <sup>b</sup>				No. of vents	Zone 9				Zone 11				Zone 67									
				Pressure (atm)					Pressure (atm)					Post temp (°C)	HM		JCS		Post temp (°C)	HM		JCS		Post temp (°C)	HM		JCS				
				H <sub>2</sub> O	H <sub>2</sub>	CO	P <sub>T</sub>		H <sub>2</sub> O	H <sub>2</sub>	CO	P <sub>T</sub>			BO	FSL <sup>c</sup>	BO	FSL		BO	FSL	BO	FSL		BO	FSL	BO	FSL			
1	1	788	584 <sup>d</sup>	1.2	0.014	50	1.2	2.7N3 <sup>e</sup>	50	780	2.6N5	4.2N5	4.5N6	7.2N6	780	2.6N5	4.2N4	4.5N6	7.2N6	780	2.6N5	4.2N5	4.5N6	7.2N6	780	2.6N5	4.2N5	4.5N6	7.2N6		
	3	788	0	2.2	0.037	45	1	2.2	7.9N5	45	780	7.8N5	1.3N4	1.4N5	2.3N5	780	7.8N5	1.3N4	1.4N5	2.3N5	780	7.8N5	1.3N4	1.4N5	2.3N5	780	7.8N5	1.3N4	1.4N5	2.3N5	
	11	521	0	1.2	0.077	26	1	1.3	0.016	26	340	2.6N4	4.2N4	4.5N5	7.2N5	386	2.6N4	4.2N4	4.5N5	7.2N5	688	2.6N4	4.3N4	4.5N5	7.2N5	688	2.6N4	4.3N4	4.5N5	7.2N5	
	21	440	0	1.1	0.070	24	1	1.1	0.014	24	293	↓	↓	↓	↓	301	↓	↓	↓	↓	547	2.9N4	4.6N4	4.6N5	7.3N5	547	2.9N4	4.6N4	4.6N5	7.3N5	
	31	420	0	1.1	0.072	24	1	1.2	0.015	24	299	↓	↓	↓	↓	306	↓	↓	↓	↓	546	↓	↓	↓	↓	546	↓	↓	↓	↓	
	41	414	0	1.2	0.076	26	1	1.2	0.015	26	329	↓	↓	↓	↓	321	↓	↓	↓	↓	538	↓	↓	↓	↓	538	↓	↓	↓	↓	
2	1	788	563 <sup>f</sup>	1.3	0.014	50	2	1.3	2.7N3	50	2	780	2.6N5	4.2N5	4.5N6	7.2N6	780	2.6N5	4.2N5	4.5N6	7.2N6	780	2.6N5	4.2N5	4.5N6	7.2N6	780	2.6N5	4.2N5	4.5N6	7.2N6
	11	774	0	11.0	0.13	49	1	11.0	0.029	49	794	5.0N4	4.8N4	5.8N5	9.3N5	787	2.9N4	4.7N4	5.6N5	9.0N5	783	2.9N4	4.7N4	5.6N5	9.0N5	783	2.9N4	4.7N4	5.6N5	9.0N5	
	21	759	0	11.0	0.23	50	1	12.0	0.045	50	808	6.7N4	1.0N3	1.6N4	2.5N4	794	6.1N4	9.6N4	1.3N4	2.0N4	786	5.7N4	9.2N4	1.1N4	1.8N4	790	5.7N4	9.2N4	1.1N4	1.8N4	
	31	745	0	10.0	0.27	45	1	10.0	0.047	45	822	1.1N3	1.8N3	3.5N4	5.1N4	801	9.7N4	1.5N3	2.2N4	3.4N4	790	8.3N4	1.4N3	2.1N4	3.2N4	790	8.3N4	1.4N3	2.1N4	3.2N4	
	41	698	0	8.8	0.27	39	1	9.0	0.044	39	691	1.8N3	2.6N3	6.3N4	8.3N4	694	1.3N3	2.1N3	5.3N4	5.1N4	780	1.2N3	1.9N3	2.5N4	3.9N4	780	1.2N3	1.9N3	2.5N4	3.9N4	
	51	651	0	7.6	0.25	34	1	7.8	0.038	34	561	↓	↓	↓	↓	587	↓	↓	↓	↓	770	1.5N3	2.3N3	2.9N4	4.7N4	770	1.5N3	2.3N3	2.9N4	4.7N4	
	61	604	0	6.4	0.21	29	1	6.6	0.032	29	431	↓	↓	↓	↓	481	↓	↓	↓	↓	760	1.7N3	2.7N3	3.2N4	5.1N4	760	1.7N3	2.7N3	3.2N4	5.1N4	
	81	539	0	5.7	0.19	25	1	5.8	0.029	26	353	↓	↓	↓	↓	381	↓	↓	↓	↓	682	1.9N3	3.0N3	3.4N4	5.5N4	682	1.9N3	3.0N3	3.4N4	5.5N4	
	3	1	788	563 <sup>f</sup>	1.3	0.014	50	2	1.3	2.7N3	50	2	780	2.6N5	4.2N5	4.5N6	7.2N6	780	2.6N5	4.2N5	4.5N6	7.2N6	780	2.6N5	4.2N5	4.5N6	7.2N6	780	2.6N5	4.2N5	4.5N6
11		804	0	12.0	0.15	51	1	12.0	0.035	51	1	838	3.6N4	5.4N4	1.1N4	1.6N4	810	3.1N4	5.0N4	6.8N5	1.1N4	785	2.9N4	4.7N4	5.5N5	9.0N5	785	2.9N4	4.7N4	5.5N5	9.0N5
21		821	0	11.0	0.36	48	1	11.0	0.11	48	895	1.5N3	1.9N3	1.1N3	1.2N3	840	8.8N4	1.3N3	2.9N4	4.1N4	790	5.9N4	3.4N4	1.4N4	1.5N4	790	5.9N4	3.4N4	1.4N4	1.5N4	
31		838	0	11.0	0.73	50	1	12.0	0.24	51	2	953	5.1N3	5.0N3	6.6N3	5.7N3	870	2.0N3	2.6N3	9.1N4	1.1N3	795	9.2N4	1.5N3	1.2N4	2.5N4	795	9.2N4	1.5N3	1.2N4	2.5N4
41		786	0	8.4	0.97	42	1	8.0	0.32	41	872	1.2N2	1.0N2	2.0N2	1.4N2	811	3.7N3	4.4N3	2.0N3	2.3N3	793	1.3N3	2.0N3	2.1N4	3.7N4	793	1.3N3	2.0N3	2.1N4	3.7N4	
51		734	0	7.7	1.0	39	1	7.4	0.31	38	790	1.5N2	1.2N2	2.1N2	1.6N2	753	4.2N3	5.1N3	2.1N3	2.4N3	792	1.6N3	2.6N3	2.6N4	4.6N4	792	1.6N3	2.6N3	2.6N4	4.6N4	
61		682	0	7.1	0.98	36	1	6.8	0.29	35	709	↓	↓	↓	↓	695	4.3N3	5.3N3	↓	↓	790	2.0N3	3.1N3	3.4N4	5.2N4	790	2.0N3	3.1N3	3.4N4	5.2N4	
81		615	0	5.6	0.78	28	1	5.3	0.23	28	497	↓	↓	↓	↓	519	↓	↓	↓	↓	759	2.5N3	3.9N3	4.0N4	6.3N4	759	2.5N3	3.9N3	4.0N4	6.3N4	
101		550	0	4.5	0.63	23	1	4.4	0.18	23	391	↓	↓	↓	↓	389	↓	↓	↓	↓	703	2.8N3	4.4N3	4.2N4	6.6N4	703	2.8N3	4.4N3	4.2N4	6.6N4	
3A		1	788	563 <sup>f</sup>	1.3	0.014	50	2	1.3	2.7N3	50	2	780	2.6N5	4.2N5	4.5N6	7.2N6	780	2.6N5	4.2N5	4.5N6	7.2N6	780	2.6N5	4.2N5	4.5N6	7.2N6	780	2.6N5	4.2N5	4.5N6
	11	812	0	12.0	0.15	51	1	12.0	0.038	51	1	830	3.4N4	5.3N4	9.5N5	1.4N4	810	3.1N4	5.0N4	6.8N5	1.1N4	782	2.8N4	4.6N4	5.8N5	8.4N5	782	2.8N4	4.6N4	5.8N5	8.4N5
	21	836	0	10.0	0.41	47	1	11.0	0.14	47	880	1.3N3	1.7N3	7.2N4	8.6N4	839	8.8N4	1.3N3	2.8N4	4.0N4	785	5.6N4	9.0N4	1.0N4	1.6N4	785	5.6N4	9.0N4	1.0N4	1.6N4	
	31	860	0	10.0	0.92	50	1	11.0	0.36	50	2	930	3.9N3	4.2N3	3.4N3	3.3N3	869	1.9N3	2.9N3	7.9N4	1.0N3	788	8.5N4	1.4N3	1.5N4	2.4N4	788	8.5N4	1.4N3	1.5N4	2.4N4
	41	849	0	9.7	1.7	50	1	8.2	0.53	49	934	9.8N3	8.5N3	9.8N3	7.9N3	875	3.8N3	4.5N3	1.8N3	1.9N3	789	1.2N3	1.9N3	1.9N4	3.0N4	789	1.2N3	1.9N3	1.9N4	3.0N4	
	51	838	0	8.0	2.0	45	1	8.1	0.68	45	939	1.6N2	1.3N2	1.5N2	1.2N2	881	5.9N3	6.6N3	2.5N3	2.8N3	790	1.5N3	2.4N3	2.6N4	3.4N4	790	1.5N3	2.4N3	2.6N4	3.4N4	
	61	827	0	7.5	2.5	46	1	8.0	0.77	46	944	2.3N2	1.8N2	2.0N2	1.5N2	887	8.2N3	8.9N3	3.4N3	3.7N3	792	1.8N3	2.9N3	2.4N4	3.9N4	792	1.8N3	2.9N3	2.4N4	3.9N4	
	81	731	0	5.9	2.5	38	1	6.6	0.69	39	740	3.1N2	2.4N2	2.5N2	1.9N2	750	1.1N2	1.2N2	4.4N2	4.6N2	789	2.5N3	3.9N3	2.0N4	4.7N4	789	2.5N3	3.9N3	2.0N4	4.7N4	
	101	657	0	4.7	2.0	31	1	5.4	0.55	32	543	3.1N2	2.4N2	2.5N2	1.9N2	535	1.1N2	1.2N2	4.4N2	4.6N2	780	3.1N3	4.9N3	2.5N4	5.4N4	780	3.1N3	4.9N3	2.5N4	5.4N4	

<sup>a</sup>Calculated assuming Helms and MacPherson corrosion equation.<sup>10</sup>

<sup>b</sup>Calculated assuming Johnstone, Chen, and Scott corrosion equation.<sup>11</sup>

<sup>c</sup>Signifies "fractional strength loss."

<sup>d</sup>Applies for first 2 min.

<sup>e</sup>Signifies  $2.7 \times 10^{-3}$ .

<sup>f</sup>Applies for first 10 min.

input core temperature history and steam ingress rates to the OXIDO program, and the resulting primary coolant composition as a function of time following tube rupture. The core temperatures listed are the reaction-average temperatures, defined in Sect. 2.2, which determine effective reactivity of the core graphite to the ingressed steam.

Columns 5 through 12 of Table 5.1 list the calculated  $H_2O$  and  $H_2$  concentrations as a function of time (CO levels are presumed to be equal to  $H_2$ ) and the total primary system pressure; first, it is assumed that a core corrosion rate according to the Helms and MacPherson<sup>10</sup> (HM) equations and, second, the Johnstone, Chen, and Scott<sup>11</sup> (JCS) corrosion expressions are assumed to apply. Columns 8 and 12 (No. of vents) indicate the venting behavior of the primary system for each case as calculated by the idealization of the vent-valve systems incorporated in the program. The numbers in these columns signify how many times the vent opens due to overpressure and subsequently closes due to pressure relief. As already noted, the precise venting behavior during these accident sequences plays only a minor role in determining core post strength loss, and little effort was expended to more realistically model venting behavior. Thus, the venting characteristics listed must be considered only as rough approximations sufficient for the present purposes (i.e., to define primary loop conditions for graphite corrosion estimates).

The right portion of Table 5.1 pertains to the condition of the core posts under refueling zones 9, 11, and 67 during each assumed accident. The temperature histories listed are those computed by ORECA-3 as representing the coolant temperature exiting from the core beneath these zones, and were assumed to represent the average or nominal core post temperatures at the indicated time in the accident sequence. The results of the burn-off and fractional strength loss calculations using OXIDO are presented in the table, again assuming both the HM corrosion equation and JCS for each refueling zone.

Tables 5.2 and 5.3 similarly show the calculated results for Cases 4 and 5, and 6 and 6A, respectively. Since these are the four assumed depressurization losses, no venting behavior is indicated.

Table 5.2. Tabulated results for Cases 4 and 5 (DBDA cases). Strength loss estimates for the nominal core post

Case	Time (min)	Reaction-ave. core temp (°C)	Steam ingress rate (mol/s)	HM <sup>a</sup>				JCS <sup>b</sup>				Zone 9				Zone 11				Zone 67				
				Pressure (atm)				Pressure (atm)				Post temp (°C)	HM		JCS		Post temp (°C)	HM		JCS		Post temp (°C)	HM	
H <sub>2</sub> O	H <sub>2</sub>	CO	P <sub>T</sub>	H <sub>2</sub> O	H <sub>2</sub>	CO	P <sub>T</sub>	BO	FSL <sup>c</sup>	BO	FSL		BO	FSL	BO	FSL		BO	FSL	BO	FSL		BO	FSL
4	1	788	548 <sup>d</sup>	0.46	1.1N3 <sup>e</sup>	4.2	0.46	1.0N3	4.2	780	8.6N6	1.4N5	4.3N6	6.8N6	780	8.6N6	1.4N5	4.3N6	6.8N6	780	8.6N6	1.4N5	4.3N6	6.8N6
	2	788	548	1.5	0.012	4.7	1.5	3.6N5	4.7	780	3.5N5	5.6N5	9.0N6	1.5N5	780	3.5N5	5.6N5	9.0N6	1.5N5	780	3.5N5	5.6N5	9.0N6	1.5N5
	3	788	0	1.2	0.023	3.9	1.3	5.6N5	3.9	780	6.1N5	9.8N5	1.4N5	2.2N5	780	6.1N5	9.8N5	1.4N5	2.2N5	780	6.1N5	9.8N5	1.4N5	2.2N5
	11	700	↓	0.53	0.072	1.9	0.57	0.014	1.9	748	2.3N4	3.7N4	4.2N5	6.7N5	761	2.3N4	3.7N4	4.2N5	6.8N5	777	2.3N4	3.8N4	4.4N5	7.0N5
	21	645	↓	0.33	0.049	1.2	0.36	9.0N3	1.2	577	2.6N4	4.3N4	4.8N5	8.0N5	632	2.7N4	4.5N4	5.4N5	9.0N5	764	3.0N4	4.9N4	7.0N5	1.1N4
	31	607	↓	0.27	0.041	1.0	0.29	7.4N3	1.0	479	↓	↓	↓	↓	543	↓	↓	↓	↓	752	3.2N4	5.3N4	5.4N5	1.4N4
	41	679	↓	0.25	0.037	0.91	0.26	6.7N3	0.92	408	↓	↓	↓	↓	466	↓	↓	↓	↓	738	3.2N4	5.5N4	8.3N5	1.6N4
	51	553	↓	0.26	0.039	0.94	0.27	6.9N3	0.95	338	↓	↓	↓	↓	372	↓	↓	↓	↓	707	3.2N4	5.6N4	4.7N5	1.6N4
5	1	788	563 <sup>f</sup>	0.47	1.2N3	4.2	0.47	1.0N3	4.2	780	9.4N6	1.5N5	4.3N6	6.9N6	780	9.4N6	1.5N5	4.3N6	6.9N6	780	9.4N6	1.5N5	4.3N6	6.9N6
	2	788	563	1.6	0.013	4.7	1.6	3.6N3	4.8	780	3.6N5	5.7N5	9.0N6	1.5N5	780	3.6N5	5.7N5	9.0N6	1.5N5	780	3.6N5	5.7N5	9.0N6	1.5N5
	11	836	0	4.0	0.080	4.5	4.0	0.032	4.6	854	3.8N4	5.5N4	1.6N4	2.0N4	824	3.2N4	4.9N4	8.1N5	1.2N4	784	2.7N4	4.4N4	5.4N5	3.7N5
	21	885	↓	1.2	0.41	2.1	1.4	0.13	2.3	928	2.2N3	2.4N3	9.6N4	1.0N3	869	1.1N3	1.5N3	3.1N4	4.0N4	789	5.6N4	8.5N4	8.3N5	1.4N4
	31	933	↓	0.31	0.66	1.7	0.55	0.24	2.0	1002	4.4N5	4.0N3	2.6N3	2.1N3	914	1.9N3	2.3N3	5.9N4	7.0N4	795	7.1N4	1.1N3	1.0N4	1.6N4
	41	933	↓	0.17	0.57	1.4	0.22	0.35	1.4	1033	4.9N5	4.2N3	4.4N3	2.9N3	955	2.0N3	2.4N3	8.6N4	9.1N4	797	7.1N4	1.1N3	1.1N4	1.7N4
	51	933	↓	0.12	0.53	1.2	0.11	0.38	1.2	1064	5.2N5	4.3N3	5.7N3	3.4N3	957	2.1N3	2.4N3	1.0N3	1.0N3	800	7.2N4	1.1N3	1.1N4	1.7N4
	61	934	↓	0.089	0.50	1.2	0.059	0.39	1.1	1095	5.5N5	4.4N3	6.6N3	3.7N3	978	2.1N3	2.5N3	1.2N3	1.1N3	804	↓	1.2N3	↓	1.5N4
	81	877	↓	0.055	0.46	1.0	0.026	0.38	1.0	1030	6.2N5	4.6N3	7.6N3	3.9N3	940	2.2N3	2.6N3	1.4N3	1.2N3	808	↓	↓	↓	↓
	101	812	↓	0.045	0.44	0.97	0.021	0.37	0.95	955	↓	↓	↓	4.0N3	876	↓	↓	↓	1.3N3	810	↓	↓	↓	↓
	121	738	↓	0.041	0.42	0.93	0.021	0.35	0.91	809	↓	↓	↓	4.0N3	830	↓	↓	↓	1.3N3	811	↓	↓	↓	↓

<sup>a</sup>Calculated assuming Helms and MacPherson corrosion equation.<sup>10</sup>

<sup>b</sup>Calculated assuming Johnstone, Chen, and Scott corrosion equation.<sup>11</sup>

<sup>c</sup>Signifies "fractional strength loss."

<sup>d</sup>Applies for first 2 min.

<sup>e</sup>Signifies  $1.1 \times 10^{-3}$ .

<sup>f</sup>Applies for first 10 min.

Table 5.3. Tabulated results for Cases 6 and 6A (DBEA cases). Strength loss estimates for nominal core posts

Case	Time (min)	Reaction-ave. core temp (°C)	Steam ingress rate (mol/s)	HM <sup>a</sup>				JCS <sup>b</sup>				Post temp (°C)	Zone 9				Post temp (°C)	Zone 11				Post temp (°C)	Zone 67						
				Pressure (atm)				Pressure (atm)					BO	HM	PSL <sup>c</sup>	BO		JCS	PSL	BO	JCS		PSL	BO	JCS	PSL			
				H <sub>2</sub> O	H <sub>2</sub>	CO	P <sub>T</sub>	H <sub>2</sub> O	H <sub>2</sub>	CO	P <sub>T</sub>																( $\frac{K}{cm^2}$ )	( $\frac{K}{cm^2}$ )	( $\frac{K}{cm^2}$ )
6	1	788	563 <sup>d</sup>	0.47	1.0M3 <sup>e</sup>	4.2	0.47	1.0M3	4.2	780	9.4M5	1.5M5	4.3M6	6.9M6	780	9.4M5	1.5M5	4.3M6	6.9M6	780	9.4M5	1.5M5	4.3M6	6.9M6	780	9.4M5	1.5M5	4.3M6	6.9M6
	2	↓	↓	1.6	0.013	4.7	1.6	3.6M3	4.8	↓	3.6M5	5.7M5	9.0M6	1.5M5	↓	3.6M5	5.7M5	9.0M6	1.5M5	↓	3.6M5	5.7M5	9.0M6	1.5M5	↓	3.6M5	5.7M5	9.0M6	1.5M5
	3	↓	↓	2.4	0.023	5.1	2.5	5.7M3	5.1	↓	6.2M5	1.0M4	1.4M5	2.2M5	↓	6.2M5	1.0M4	1.4M5	2.2M5	↓	6.2M5	1.0M4	1.4M5	2.2M5	↓	6.2M5	1.0M4	1.4M5	2.2M5
	11	852	0	3.9	0.094	4.5	3.9	0.048	4.6	842	3.5M4	5.2M4	1.6M4	2.2M4	818	3.1M4	4.8M4	7.3M5	1.1M4	783	2.7M4	4.0M4	5.3M5	8.6M5	783	2.7M4	4.0M4	5.3M5	8.6M5
	21	916	↓	0.92	0.60	2.3	1.2	0.19	2.6	904	1.6M3	2.0M3	5.0M4	5.8M4	856	1.0M3	1.4M3	2.1M4	2.9M4	787	5.6M4	8.3M4	8.1M5	1.3M4	787	5.6M4	8.3M4	8.1M5	1.3M4
	31	980	↓	0.24	0.68	1.7	0.37	0.35	1.9	967	2.3M3	2.5M3	1.0M3	1.0M3	894	1.3M3	1.7M3	3.1M4	4.1M4	791	6.1M4	9.5M4	8.0M5	1.4M4	791	6.1M4	9.5M4	8.0M5	1.4M4
	41	1005	↓	0.092	0.62	1.4	0.065	0.49	1.4	1025	2.4M3	2.6M3	1.4M3	1.2M3	923	1.0M3	1.4M3	3.7M4	4.6M4	795	6.2M4	9.6M4	9.0M5	1.4M4	795	6.2M4	9.6M4	9.0M5	1.4M4
	61	1056	↓	-	-	1.2	1.1M4	0.45	1.2	1142	↓	↓	↓	↓	1012	↓	↓	↓	↓	803	↓	↓	↓	↓	803	↓	↓	↓	↓
	81	1063	↓	-	-	1.2	6.5M10	0.39	1.2	1229	↓	↓	↓	↓	1073	↓	↓	↓	↓	810	↓	↓	↓	↓	810	↓	↓	↓	↓
	101	1064	↓	-	-	1.2	9.7M17	0.34	1.2	1280	↓	↓	↓	↓	1108	↓	↓	↓	↓	816	↓	↓	↓	↓	816	↓	↓	↓	↓
6A	1	788	563 <sup>d</sup>	0.47	1.2M3	4.2	0.47	1.0M3	4.2	780	9.4M5	1.5M5	4.3M6	6.9M6	780	9.4M5	1.5M5	4.3M6	6.9M6	780	9.4M5	1.5M5	4.3M6	6.9M6	780	9.4M5	1.5M5	4.3M6	6.9M6
	2	↓	↓	1.6	0.013	4.7	1.6	3.6M3	4.8	↓	3.6M5	5.7M5	9.0M6	1.4M5	↓	3.6M5	5.7M5	9.0M6	1.5M5	↓	3.6M5	5.7M5	8.6M6	1.4M5	↓	3.6M5	5.7M5	8.6M6	1.4M5
	3	↓	↓	2.4	0.023	5.1	2.5	5.7M3	5.1	↓	6.2M5	1.0M4	1.4M5	2.2M5	↓	6.2M5	1.0M4	1.4M5	2.2M5	↓	6.2M5	1.0M4	1.3M5	2.2M5	↓	6.2M5	1.0M4	1.3M5	2.2M5
	11	827	0	3.9	0.071	4.4	3.9	0.024	4.5	809	3.0M4	4.7M4	6.6M5	1.0M4	798	2.8M4	4.5M4	5.9M5	5.4M5	781	2.6M4	4.3M4	5.1M5	8.2M5	781	2.6M4	4.3M4	5.1M5	8.2M5
	21	865	↓	1.2	0.31	2.0	1.4	0.095	2.2	838	2.5M4	1.2M3	1.9M4	2.8M4	815	7.0M4	1.1M3	1.3M4	2.1M4	761	5.3M4	8.5M4	8.3M5	1.3M4	761	5.3M4	8.5M4	8.3M5	1.3M4
	31	904	↓	0.38	0.60	1.7	0.65	0.17	2.0	867	1.3M3	2.0M3	3.2M4	4.4M4	832	1.1M3	1.6M3	1.9M4	2.8M4	782	7.0M4	1.1M3	9.6M5	1.6M4	782	7.0M4	1.1M3	9.6M5	1.6M4
	41	932	↓	0.21	0.55	1.4	0.32	0.26	1.5	900	1.5M3	2.1M3	4.4M4	5.6M4	854	1.1M3	1.6M3	2.2M4	3.2M4	784	7.1M4	1.2M3	1.0M4	1.6M4	784	7.1M4	1.2M3	1.0M4	1.6M4
	61	988	↓	0.089	0.51	1.2	0.047	0.40	1.1	964	1.6M3	2.1M3	6.5M4	7.2M4	897	1.2M3	1.7M3	2.7M4	3.7M4	787	↓	↓	↓	↓	787	↓	↓	↓	↓
	81	1025	↓	0.2M3	0.53	1.1	5.7M4	0.42	1.1	1031	1.7M3	2.2M3	7.1M4	7.6M4	943	↓	↓	↓	↓	791	↓	↓	↓	↓	791	↓	↓	↓	↓
	101	1056	↓	-	-	1.1	1.3M7	0.30	1.1	1097	1.7M3	2.2M3	7.1M4	7.6M4	989	↓	↓	↓	↓	795	↓	↓	↓	↓	795	↓	↓	↓	↓

<sup>a</sup>Calculated assuming Helms and MacPherson corrosion equation.

<sup>b</sup>Calculated assuming Johnstone, Chen, and Scott corrosion equation.

<sup>c</sup>Signifies "Fractional strength loss."

<sup>d</sup>Applies for first 10 min.

<sup>e</sup>Signifies  $1.0 \times 10^{-3}$ .

Pertinent results for the Case 1 event are graphically illustrated in Fig. 5.1. Note that under the conditions of this event, the HM corrosion equation predicts a strength loss about six times higher than that predicted by the JCS equation, the higher estimate being about 0.04% and the lower 0.007%. The strength losses incurred reach their maximum level about 15 min into the incident. The lower portion of the figure illustrates the total pressure and coolant composition behavior as a function of time. Since predictions for the total pressure and for the steam partial pressure are very close using either the HM or JCS equations, they are shown on one line. The partial pressure of  $H_2$  shown in the figure pertains to the HM-predicted value; the JCS value (not shown) is about a factor of 5 lower, reflecting the lower rates predicted by JCS for this case. The steam pressure peaks at 2.2 atm about 3 min after tube failure.

Results for the Case 2 event are illustrated in Fig. 5.2. Higher strength losses are again predicted by the HM equation, but only by a factor of  $\sim 3$  instead of 6 as for the previous case. Some differentiation occurs between the three typical core locations selected for analysis; however, the range is still small. Strength losses appear to level out at about 0.25% about 95 min after tube failure assuming the HM equation, and at about 0.06% assuming the JCS rate equation. Again, the lower portion of Fig. 5.2 illustrates the total pressure and composition.

Figure 5.3 illustrates the calculated results for Case 3A, which showed similar trends to Case 3 (not shown) but with somewhat higher estimated strength losses. The region of highest radial power factor, zone 9, clearly shows the highest degree of strength loss, leveling out between 1.9 and 2.4% about 80 min following tube failure. Substantially lower strength losses are predicted for the nominal post in zone 67, a peripheral zone, while the results for zone 11, selected as an "average" region fall in between. Curves for the pressure histories indicate a hydrogen and carbon monoxide buildup of 0.8 to 2.5 atm, as predicted by using the JCS and HM equations, respectively. Predicted total pressure and steam partial pressure levels do not differ greatly from those predicted for Case 2.

Figures 5.4-5.6 show the calculated results for the three depressurization cases 4, 5, and 6. Case 6A results, which are not shown, are similar

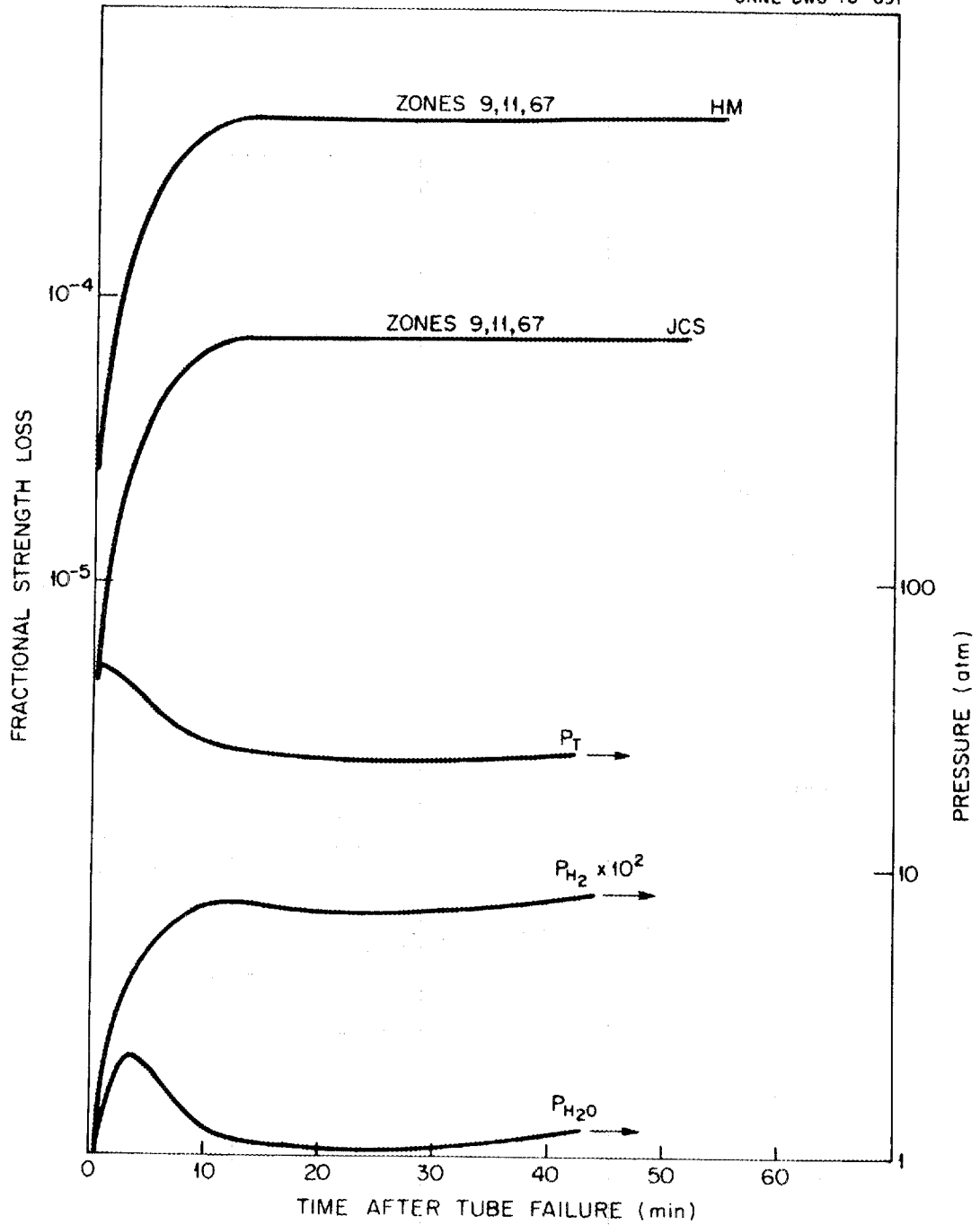


Fig. 5.1. Case 1 event. Predicted strength loss for the nominal core post and primary coolant pressure history.

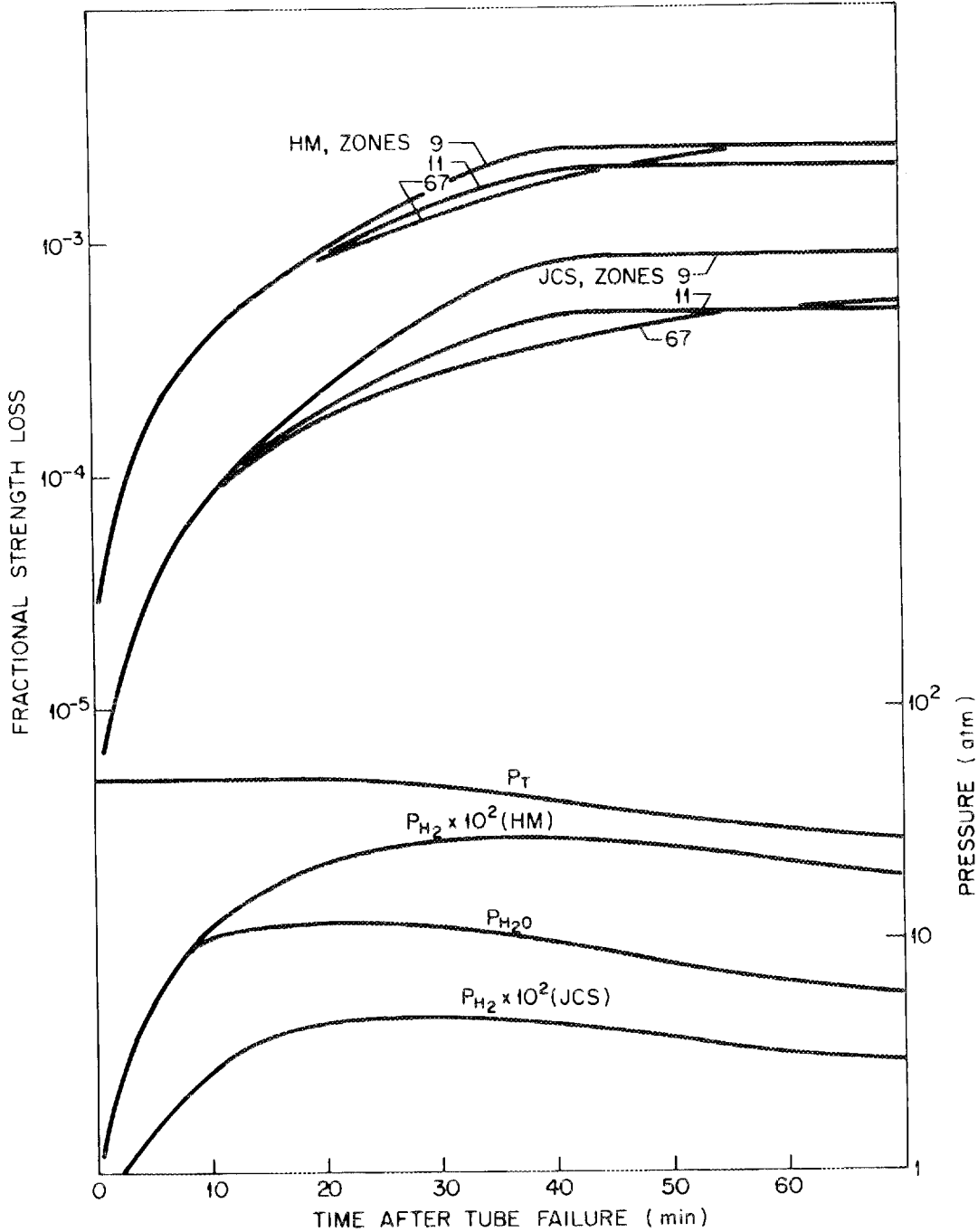


Fig. 5.2. Case 2 event. Predicted strength losses of the nominal core posts and primary coolant pressure history.

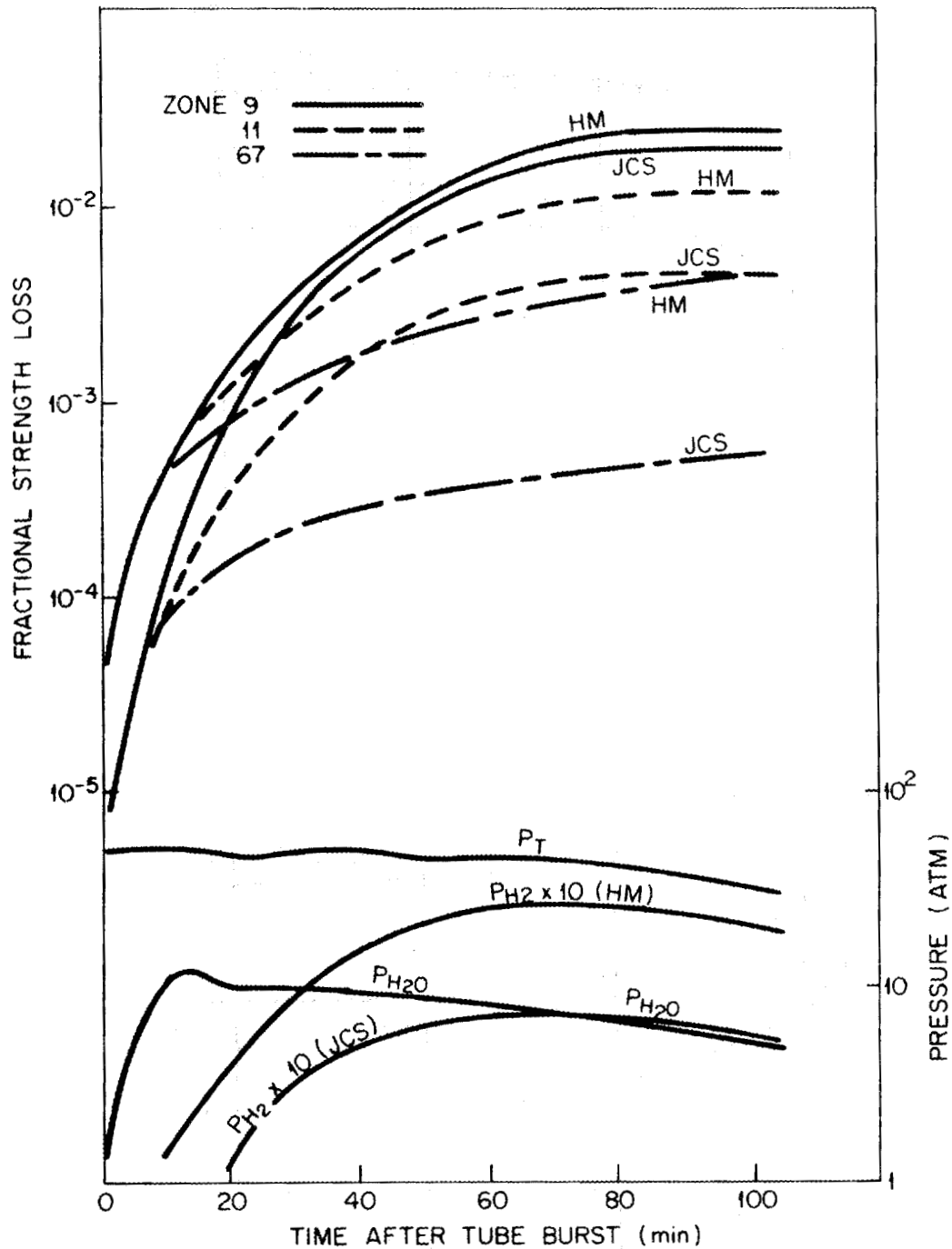


Fig. 5.3. Case 3A event. Predicted strength losses for the nominal core posts and primary coolant pressure history.

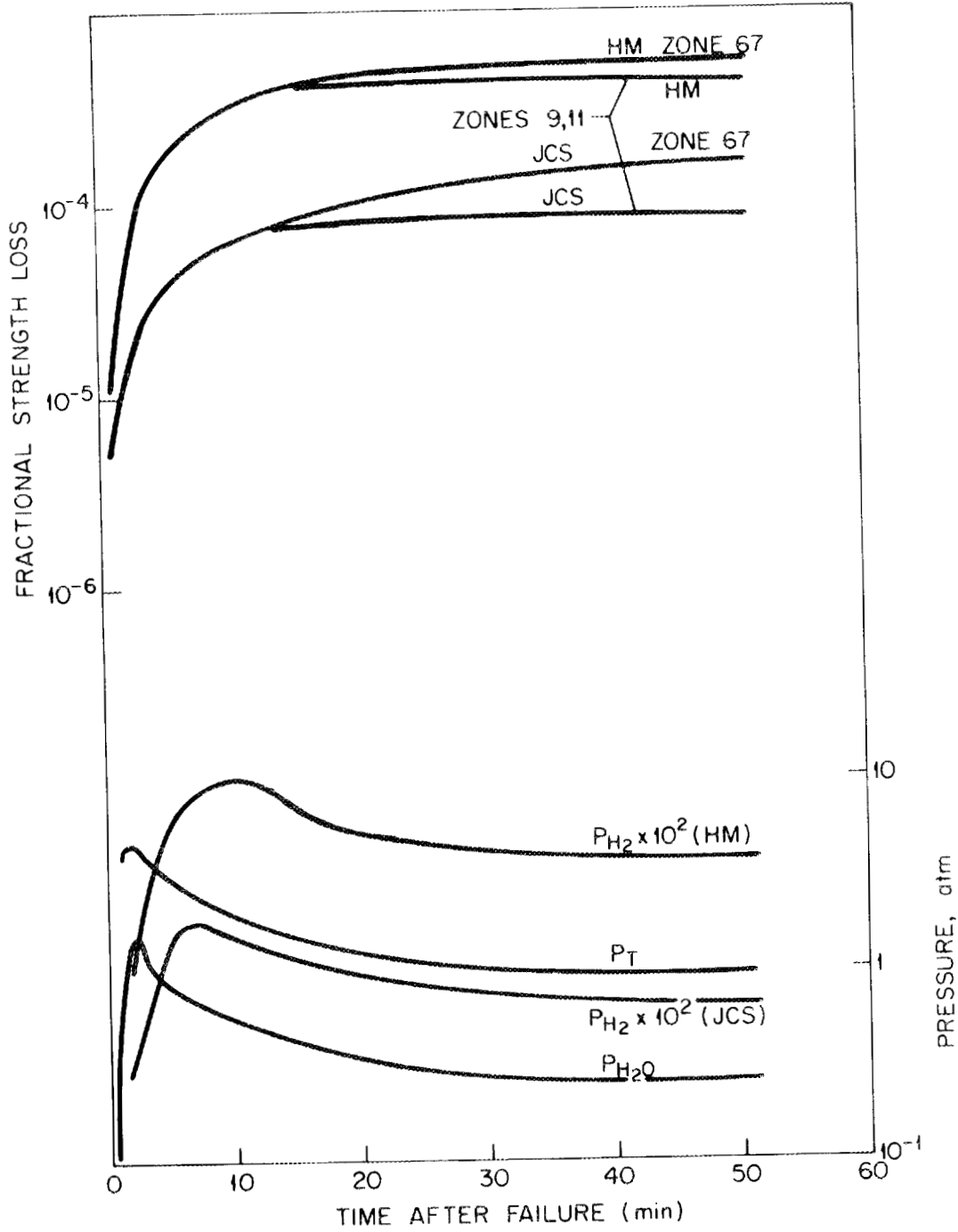


Fig. 5.4. Case 4 event. Predicted fractional core post strength loss and primary history.

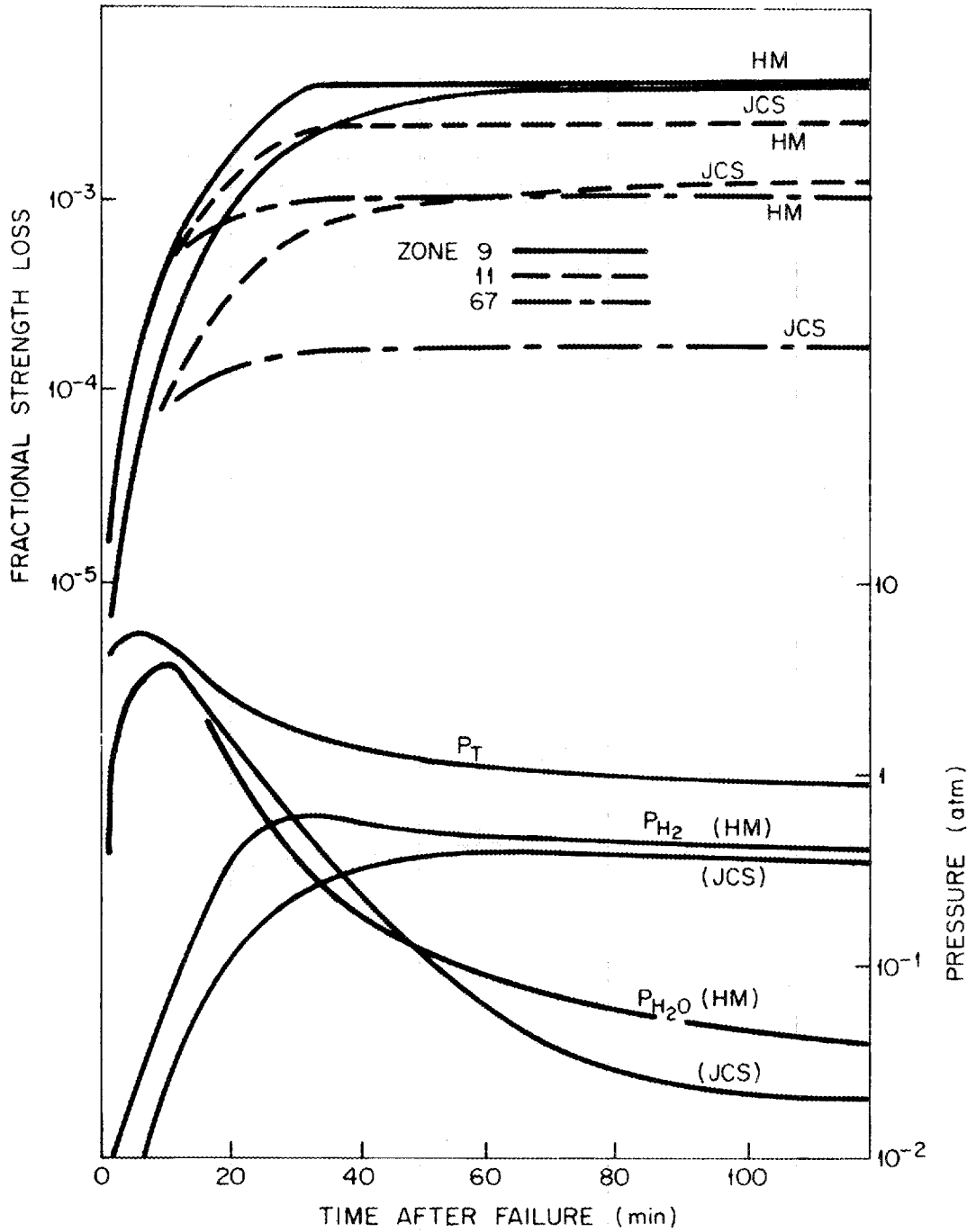


Fig. 5.5. Case 5 event. Predicted fractional core post strength loss and pressure history.

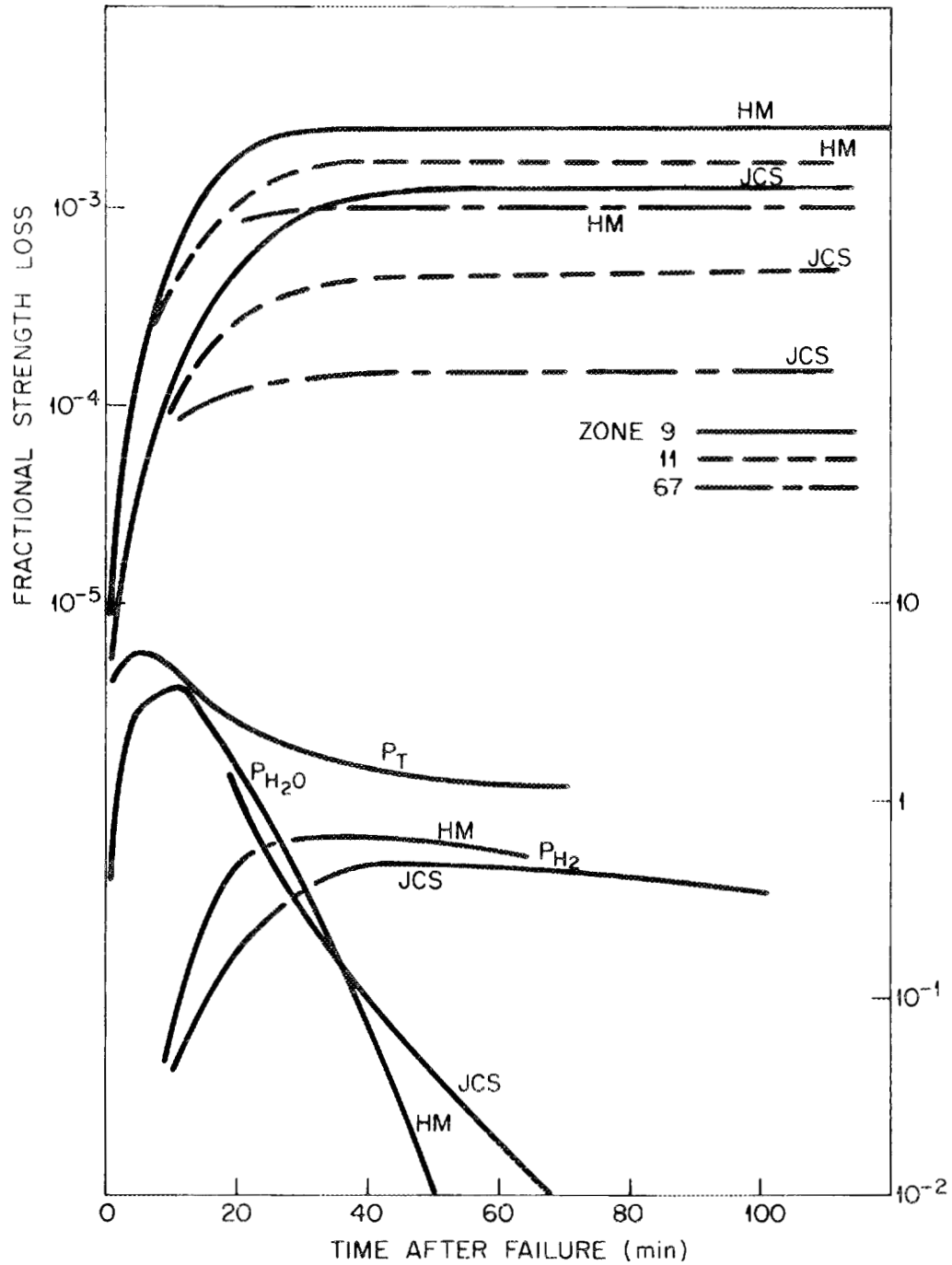


Fig. 5.6. Case 6 event. Predicted fractional core post strength loss and pressure history.

to Case 6. These cases differ from those illustrated in Figs. 5.1-5.3 by the rapid pressure fall to 1 atm due to the depressurization blowdown, which also serves to reduce the accumulated levels of  $H_2O$ ,  $H_2$ , and  $CO$ . Hence, the effect of higher temperatures experienced by the core posts during the assumed depressurization events are partially offset by reductions in oxidant concentrations resulting from the blowdown. It is interesting to note that the predicted strength loss for the nominal core post on the periphery in Fig. 5.4 exceeds the estimated loss for the interior zones, 9 and 11, as a result of the Case 4 event. This was the only case where this occurred. As noted in Sect. 2, the peripheral zones are characterized by a smaller temperature excursion of a longer duration following a tube burst event.

Results presented in Sect. 5.1 are summarized briefly in Table 5.4. The maximum predicted effect occurs under zone 9 in Case 3A, where it is predicted that the incurred strength loss would range from 2.4 to 1.9% for the nominal post. The maximum predicted partial pressures of  $H_2O$ ,  $H_2$ , and  $CO$  for each of the eight assumed accident events are also listed in the table.

## 5.2 Effect of Localized Temperature Excess on Estimated Strength Loss

One of the principal conclusions in Part I of this study relating to steady state operation was that localized zones of temperature excess in the core post regions are a significant factor in determining strength loss rates due to steam ingress. It was estimated that a core post at the nominal coolant outlet temperature would have zero probability of experiencing 50% strength loss as a result of full-life exposure to the maximum steam concentrations allowable under continuous operations. On the other hand, the same post exposed at 90°C higher temperature would be virtually assured of 50% strength at the same oxidant concentration. It is therefore incumbent to examine this effect for the case of shutdown transients.

At the time of the steady-state analysis, it was judged on the basis of available hot-streaking and operation limits information that a

Table 5.4. Predicted strength losses incurred by the nominal support posts beneath zones 9, 11, and 67, and the maximum partial pressures of steam and H<sub>2</sub> calculated using  $\phi$ XIDO

Case <sup>a</sup>	Maximum		Strength loss (%) of nominal core post beneath:		
	P(H <sub>2</sub> O) (atm)	P(H <sub>2</sub> , CO) (atm)	Zone 9	Zone 11	Zone 67
1	2.2	0.08-0.02 <sup>b</sup>	0.042-0.007 <sup>b</sup>	0.042-0.007	0.046-0.007
2	9.0	0.3 - 0.05	0.26 - 0.088	0.21 - 0.051	0.19 - 0.039
3	12.0	1.0 - 0.3	1.2 - 1.6	0.54 - 0.25	0.44 - 0.066
3A	12.0	2.5 - 0.8	2.4 - 1.9	1.2 - 0.46	0.66 - 0.062
4	1.5	0.07-0.01	0.043-0.008	0.045-0.009	0.056-0.016
5	4.0	0.7 - 0.4	0.43 - 0.40	0.26 - 0.13	0.12 - 0.018
6	2.4	0.7 - 0.4	0.26 - 0.13	0.17 - 0.046	0.12 - 0.017
6A	3.9	0.6 - 0.4	0.22 - 0.076	0.17 - 0.038	

<sup>a</sup>Cases are described in Sect. 2.1.

<sup>b</sup>First value is obtained by assuming the Helms-MacPherson corrosion rate equation; the second value assumes the Johnstone, Chen, and Scott corrosion rate equation.

reasonable estimate for a continuous, significantly large, hot spot in the core post region was 90°C. Since then, an ongoing task at GAC has attempted to fix the hot-spot situation in the core post region with more certainty. The present status of this work is mentioned in order to obtain an estimate of hot-spot effects under transient shutdown conditions.

### 5.2.1 Hot spots in the core support post at steady state

Work is currently in progress at GAC to realistically determine the extent of nonideal temperatures in the core post region. Only the preliminary results summarized in Table 5.5 are now available.

Table 5.5. Core support post temperature probability distributions under normal operating conditions<sup>13</sup>

<u>Steady state, 68% of life</u>	<u>2σ limits (°C)</u>
Region outlet thermocouple uncertainty	± 25
Region outlet control band	-83/+25
Average core outlet variation	± 20
	} ± 41
<u>Steady state with column streaking, 25% of life</u>	
Region outlet thermocouple uncertainty	± 25
Region outlet control bank	-83/+25
Average core outlet variation	± 20
Column streaking	± 109
	} ± 116
<u>Load following transient, 7% of life</u>	
(Effective for central column of high radial power factor zone)	+ 377

As Table 5.5 indicates, five factors affecting core post temperature nonidealities were considered in this preliminary study.<sup>13</sup> Under normal steady state operations, expected to occur 68% of the time, temperature deviations beneath a refueling zone were considered to be caused by (1) uncertainty in the region outlet temperature reading, (2) inaccurate flow control setting, and (3) deviation of the mean outlet coolant

temperature. The contribution of each effect is given as the  $2\sigma$  limit; that is, the extent of each deviation is expected to be within the stated range with 95% certainty. The combined effect of these three factors, obtained by taking the square root of the sum of the squares, yields a net effect of  $\pm 41^\circ\text{C}$  for this steady state condition. For this 68% of its life, the exit coolant temperature from a refueling zone is expected to lie within  $41^\circ\text{C}$  of normal 95% of the time.

The second condition referred to in Table 5.5, "Steady state with column streaking," is attributed to the augmented heating rates predicted by neutronics calculation for the central column of some refueling zones for the first year of the 4-year life of the zone. The deviation range is given as  $\pm 109^\circ\text{C}$ ; however, since this effect may be calculated and predicted, treating this factor as a random effect (such as a thermocouple uncertainty) may not be completely appropriate. The augmented power density in the central column of some refueling zones during this first year of life results in higher exit coolant temperatures from the column, which tend to be maintained over some portions of the support posts beneath the region in question. This effect, together with the other three cited causes of hot spots, yields a combined temperature range of  $\pm 116^\circ\text{C}$  for the 25% period of total life.

Finally, Table 5.5 lists the estimated temperature excess as a result of loading following transients, which is anticipated to occur during 7% of reactor life. Localized temperature elevations may occur as the reactor power level is increased to follow a load change, due to the insertion of reactivity to overcome xenon buildup. The temperature elevation cited,  $337^\circ\text{C}$ , represents the worst case caused by power peaking in the central column of the highest radial power factor zone under conditions of maximum xenon override.

### 5.2.2 Core post hot spots during tube burst shutdown transients

In applying the above discussion to the consideration of hot-spot factors during shutdown transients, one must weigh the following considerations:

1. The shutdown transient may start at the least propitious time; that is, at a time when the various factors contributing to localized overheating under steady state operations are at their worst. For example, there is a 7% chance that a tube burst event, if it occurs, would occur during a load following transient.
2. The power level during the shutdown period is extremely small as compared with the steady state level which initially created the hot zones. This would tend to relieve the temperature nonideality during shutdown. On the other hand, the existence of the hot zone at the time of reactor trip would have an effect into the shutdown transient by virtue of the sensible heat stored in the hot graphite column.
3. Since the coolant flows are much lower during shutdown (but still far into the turbulent region in the subcore region), the intensity of turbulent mixing will be correspondingly lower. This would tend to enhance hot streaking (i.e., the tendency to maintain a localized temperature excess within a flowing fluid). In opposition to this is the fact that lower flows allow more time for dispersion to occur between two set locations. In fact, it may be shown that these two tendencies cancel each other to a first approximation. Hence, as long as the flows remain within the same qualitative category, hot-streaking tendencies should remain approximately equivalent as the coolant flowrate is reduced to shutdown level.
4. Subtracting the given average core temperature variation of  $\pm 20^\circ\text{C}$  from the "steady-state temperature excess," reduces it to  $\pm 35^\circ\text{C}$  (from  $\pm 41^\circ\text{C}$ ).\* The "steady-state with column streaking" temperature excess is hardly altered,

---

\* It was shown in Sect. 6.4 of ref. 1 that core post strength loss rates were relatively insensitive to small changes in general temperature level. Only localized departures from the mean were significant.

while the "load-following hot streak" is reduced to 317°C (from 337°C) by ignoring the allowable deviation in average temperature.

It is apparent that a complete, quantitative evaluation of hot-spot effects during shutdown transients involve complex operational, neutronic, and hydrodynamic phenomena, the resolution of which is beyond the scope of this study. However, the approximate importance of this effect will be assessed by running the following two cases which appear to be reasonably representative.

Hot-spot Case 1. This case is less severe, but more probable than Case 2, below. An initial hot-streak value of 116°C is assumed, applicable to the central column of the high radial power factor zones during their initial year of service. The column streak is assumed to pass linearly to zero at the end of the shutdown.

Hot-spot Case 2. The tube failure is assumed to occur during a load following transient (7% probability). The central column hot streak for the highest radial power factor fuel zones is initially 317°C. It is assumed that the column hot streak is reduced linearly with time such that it is zero by the end of the shutdown transient.

The results for hot-spot Cases 1 and 2 are shown in Table 5.6 and are compared with the strength loss estimate for the nominal posts given previously. These estimates all refer to the posts beneath zone 9, which is the highest radial power factor zone. For hot spot Case 1, estimated strength losses for localized areas are higher by factors of about 3 to 6 assuming corrosion rates according to Helms and MacPherson,<sup>10</sup> and from about 4 to 30 according to Johnstone, Chen, and Scott.<sup>11</sup> As before, the depressurization cases result in surprisingly low strength loss estimates despite the high transient temperature situation. Case 3A results in the highest strength loss estimate, ranging from 6.8 to 12%, as a result of localized overheating.

Localized strength losses incurred as a result of assumed hot-spot Case 2 are given in the last column of Table 5.6. These range from 0 to 1.5% for Case 1 (which presumes proper operation of moisture monitor and

Table 5.6. Effect of localized hot spots on strength loss beneath a high radial power factor zone (zone 9)

Case	Strength loss (%) beneath high power factor zone 9		
	Nominal core post	Hot spot, Case 1	Hot spot, Case 2
1	0.042-0.007 <sup>a</sup>	0.24-0.23 <sup>a</sup>	1.5-0.98 <sup>a</sup>
2	0.26 - 0.088	1.2 - 2.4	6.7-19
3	1.2 - 1.6	3.8 - 9.2	8.1-24
3A	2.4 - 1.9	6.8 - 12	25.0-33
4	0.043-0.008	0.25-0.22	1.4-0.69
5	0.43 - 0.40	1.5 - 1.7	6.7-3.9
6	0.26 - 0.13	1.1 - 1.2	4.8-3.2
6A	0.22 - 0.76	1.1 - 1.1	5.0-3.5

<sup>a</sup>The first value was computed by assuming the Helms-MacPherson corrosion expression; the second value assumes the Johnstone, Chen, and Scott expression.

isolation systems following tube failure) to 25 to 33% for Case 3A, (which assumes failure to isolate and partial failure for the CACS system). Localized strength loss incurred during depressurization events range from 0.7 to 1.4% for Case 4 up to 3.5 to 5% for Case 6A.

## 6. REFERENCES

1. R. P. Wichner, Effect of Steam Corrosion on Core Post Strength Loss: I. Case of Low, Chronic Steam Ingress Rates, ORNL/TM-5534 (October 1976).
2. General Atomic Standard Safety Analysis Report (GASSAR-6), GA-A-13200.
3. S. J. Ball, ORECA-1: A Digital Computer Code for Simulating HTGR Thermal Transients, ORNL/TM-5159 (April 1976).
4. S. J. Ball, personal communication, Feb. 9, 1976.
5. R. W. Schleicher et al., An Analysis of HTGR Core Cooling Capability, LTR-1 (Mar. 30, 1973).

6. R. E. Sund, Afterheat Calculations for the HTGR, GA-LTR-4A (July 1974).
7. A. W. Barsell and M. B. Peroomian, Consequences of Water Ingress Into the HTGR Primary Coolant, GA-A13171, Fig. 2-7 (April 1975).
8. R. C. Gwaltney, Reactor Division, ORNL, personal communication, March 25, 1976.
9. E. Wicke et al., Corrosion Rate of Graphites by CO<sub>2</sub> and H<sub>2</sub>O, D.P. Rept. 391 (January 1966).
10. R. E. Helms and R. E. MacPherson, Reaction of Steam with Large Specimens of Graphite for the EGCR, ORNL/TM-1430 (March 1966).
11. H. F. Johnstone, C. Y. Chen, and D. S. Scott, "Kinetics of the Steam-Carbon Reaction in Graphite Tubes," *Ind. Eng. Chem.* 44, 1564-69 (1952).
12. J. D. Blackwood and F. McGrory, "The Carbon-Steam Reaction at High Pressure," *Aust. J. Chem.* 11, 16-33 (1958).
13. P. Havde, GAC, personal communication, May 12, 1976, Bethesda, Md. (presentation to NRC).

## INTERNAL DISTRIBUTION

- |        |                  |        |                               |
|--------|------------------|--------|-------------------------------|
| 1.     | J. L. Anderson   | 45.    | R. A. Lorenz                  |
| 2.     | S. J. Ball       | 46.    | A. L. Lotts                   |
| 3.     | D. E. Bartine    | 47.    | R. E. MacPherson              |
| 4.     | C. D. Baumann    | 48.    | J. C. Mailen                  |
| 5.     | R. L. Beatty     | 49.    | A. P. Malinauskas             |
| 6.     | J. P. Callahan   | 50.    | W. R. Martin                  |
| 7.     | D. O. Campbell   | 51.    | W. J. McDowell                |
| 8.     | D. A. Canonic    | 52.    | K. J. Notz                    |
| 9.     | C. E. Clifford   | 53.    | L. C. Oaks                    |
| 10.    | J. A. Conlin     | 54.    | A. R. Olsen                   |
| 11.    | J. H. Coobs      | 55.    | G. W. Parker                  |
| 12.    | D. A. Costanze   | 56.    | W. H. Pechin                  |
| 13.    | F. C. Davis      | 57.    | H. Postma                     |
| 14.    | J. R. DiStefano  | 58.    | R. H. Rainey                  |
| 15.    | B. C. Duggins    | 59.    | D. P. Reid                    |
| 16.    | W. P. Eatherly   | 60.    | A. D. Ryon                    |
| 17.    | D. E. Ferguson   | 61.    | J. P. Sanders                 |
| 18.    | Uri Gat          | 62.    | Dunlap Scott                  |
| 19.    | J. H. Goode      | 63.    | J. D. Sease                   |
| 20.    | A. G. Grindell   | 64.    | J. H. Shaffer                 |
| 21.    | W. S. Groenier   | 65.    | R. L. Shepard                 |
| 22.    | P. A. Haas       | 66.    | W. J. Snider                  |
| 23.    | W. R. Hamel      | 67.    | P. R. Stein                   |
| 24.    | F. E. Harrington | 68.    | R. S. Stone                   |
| 25.    | C. C. Haws       | 69.    | M. L. Tobias                  |
| 26.    | L. C. Hensley    | 70.    | D. B. Trauger                 |
| 27.    | R. M. Hill, Jr.  | 71.    | J. E. Van Cleve               |
| 28.    | F. J. Homan      | 72.    | V. C. A. Vaughen              |
| 29.    | J. R. Horton     | 73-82. | R. P. Wichner                 |
| 30.    | Vivian Jacobs    | 83.    | R. G. Wymer                   |
| 31.    | J. D. Jenkins    | 84-85. | Central Research Library      |
| 32.    | D. R. Johnson    | 86.    | Document Reference Section    |
| 33-40. | P. R. Kasten     | 87.    | Laboratory Records, ORNL-RC   |
| 41.    | W. J. Lackey     | 88-97. | Laboratory Records            |
| 42.    | K. H. Lin        | 98.    | E. L. Gaden, Jr. (consultant) |
| 43.    | T. B. Lindemer   | 99.    | C. H. Ice (consultant)        |
| 44.    | E. L. Long, Jr.  | 100.   | R. B. Richards (consultant)   |

## EXTERNAL DISTRIBUTION

101. Research and Technical Support Division, ERDA-ORO, P. O. Box E, Oak Ridge, Tn. 37830
102. Director, Reactor Division, ERDA-ORO, P. O. Box E, Oak Ridge, Tn. 37830
- 103-104. Director, Division of Nuclear Fuel Cycle and Production, ERDA, Washington, D.C. 20545
- 105-106. Director, Division of Reactor Research and Development, ERDA, Washington, D.C. 30545
- 107-282. Given distribution as shown in TID-4500 under category UC-77 -- Gas-Cooled Reactor Technology